Universidad Autónoma de Madrid
Departamento de Física Teórica
Instituto de Física Teórica

Neutrino physics in SuperK-Gd

by

Diego José González Vizoso

diegoj.gonzalez@estudiante.uam.es

Supervisor: Prof. Luis Labarga Echeverría

luis.labarga@uam.es

Master's Programme in Theoretical Physics
Elementary Particles & Cosmology
Thesis, 2019−2020

Abstract

Dissolving gadolinium salt in water Cherenkov detectors allows for very efficient neutron tagging, which opens up a vast and extremely interesting new range of measurements. By detecting free neutrons inside the detector volume one can almost univocally identify inverse beta processes from antineutrinos and thus accessing to the otherwise background whipped Diffuse Supernova Neutrino Background. Also because of the inverse beta measurement, neutron tagging makes water Cherenkov detectors excellent tools to analyze antineutrinos from nuclear power reactors. In addition to that, neutron tagging increases the detector's ability to discriminate between neutrinos and antineutrinos as their interactions in water typically feature different numbers of neutrons in their final states.

The SuperK-Gd project consists on dissolving 100 tons of ultrapure gadolinium salt in the Super Kamiokande water tank up to a final neutron tagging efficiency of $\sim$90%. As the salt is distributed uniformly along the whole fiducial volume of the experiment, one has to be extremely careful about its possible radioactive contamination. Alphas, betas and gammas from radioactive isotopes could jeopardize the physics program of SuperK-Gd. We have been responsible of the screening of about 50% of a total of 14 tons of $Gd_2(SO_4)_3$ which will be dissolved in SK during the next month. Our measurements have been performed mostly at the Canfranc Underground Laboratory.

In this thesis we introduce neutrino physics focusing mostly on the Super Kamiokande experimental program. We detail the SuperK-Gd project and its physics. We explain and thoroughly discuss our radiopurity measurements and the impact of our results on the course of the experiment.

Contents

Chapter 1

Introduction

1.1 Research Problem

By raw number of particles in the Universe, neutrinos are probably second only to photons. Every second, several trillion of them pass through us and yet they remain as one of the least known sectors in the standard model.

Water Cherenkov detectors are an invaluable tool for studying neutrinos in the range from MeV to a hundred of GeV, like solar and atmospheric. They have already shown to be capable of detecting and pointing to supernova events up to a few degrees, proven three flavour oscillations in solar and atmospheric neutrinos, measured their parameters and established bounds to proton decay lifetimes. The **Super Kamiokande** detector in Japan is the sucessor of Kamiokande and after two decades of data taking it has already made breakthroughs in the field, being the discovery of massive character of neutrinos the most relevant one. New projects like Hyper Kamiokande will continue this the trend of making a new, bigger and more precise detector.

Dissolving **gadolinium** in Super Kamiokande enables the detection of free neutrons in the water tank, which can be used to **distinguish antineutrinos from neutrinos** in the low energy range. With this upgrade, the diffuse supernova neutrino background −which are neutrinos from past supernova events− is expected to be measured. Neutron tagging is also incredibly useful in the determination of the CP violating angle δ_{CP} and mass hierarchy among other searches.

This is the reasoning behind **SuperK-Gd**, a project in which 100 tons of ultrapure gadolinium salt will be dissolved in Super Kamiokande. While the physics potential is vast, the upgrade isn't free of challenges. Past R&D projects like EGADS have evaluated the feasibility of dissolving gadolinium in water Cherenkov detectors with much success. Radiopurity measurements of the salt are very strict in order not to contaminate the water tank with impurities which could increase the background of the experiment, which needs to be close to zero for measurements of solar neutrinos, among others, not to be spoiled.

1.2 Aim and Scope

The SuperK-Gd project is already approved and underway. The intent of this thesis is to give an **overview** of neutrino physics, not only on the topics strictly related to SuperK-Gd but to also give a more broad view of their properties and the different sources. In addition to that, the **Super Kamiokande** and **SuperK-Gd projects are explained** for a public who is interested in the physics behind them but doesn't need too much details about the inner workings (e.g. technical details, energy reconstruction procedures, precise background estimations). Thus, a more didactic approach has been taken, trying to simplify and condense the most important concepts. Finally, the **radiopurity measurements** which have been realized along the past year are presented and analyzed, showing how they have impacted the future course of the experiment.

1.3 Author contributions

Having been in operation for more than 20 years, Super Kamiokande is already a well established experiment and thus many of the analysis techniques are very mature, so there is no need to redo simulations or reconstruction algorithms. It is important to identify my (the author's) personal contributions to the experiment.

For SuperK-Gd, radiopurity measurements and analyses are required, and I have been responsible of **analysing 15 samples**, several times each sample since preliminar studies are also required. I have presented updates on these measurements in **21 bi-weekly meetings** of the working group. I have also constributed to the realization of the measurements at the Canfranc Underground Laboratory. One month of presential work in Kamioka in April was planned for the Gd loading, however due to Covid-19 our flights and reservations had to be cancelled.

1.4 Outline of the Thesis

In Chapter 2, the foundations of neutrino physics and oscillations are sketched. In Chapter 3 the different neutrino sources, properties and experiments used to measure them are shown. In Chapter 4 the Super Kamiokande experiment is detailed, together with its contributions to physics as well as the potential of the new SuperK-Gd project. In Chapter 5 the basics of radiopurity techniques and procedures are developed, and our measurements shown and analyzed.

1.5 Acknowledgements

I want to thank my supervisor Luis Labarga for his experienced advice which has made this thesis possible. I am also thankful to Iulian Bandac and Javier Pérez for their work on the Canfranc Underground Laboratory and in particular on the HPGe measurements, whose analysis is in this thesis presented.

The research conducted on this thesis has been partially done with financing of the Universidad Autónoma de Madrid, "Beca de fomento de la investigación" during the years 2019 and 2020.

Chapter 2

Foundations of neutrino physics

The physics of neutrinos has now 90 years of history, in which many different developments have happened. Without delving too deep into the historical details, the foundational experiments of neutrino physics are explained, as well as the current accepted theoretical model: three flavour oscillations. The current state of neutrino parameter measurements is shown.

2.1 An elusive particle

In the late 1920's, even after crucial theories in modern physics like relativistic quantum mechanics were rising, the understanding of the atom was still lacking [17]. Atoms were thought to be composed only of protons and electrons, which existed both inside the nucleus (ejected in beta decay) and atomic electrons, around the nucleus. Of course the electron energy was expected to be monochromatic so after 20 years of beta decay measurements, the continuous spectrum and energy values of the emitted radiation couldn't be explained. Two proposals arose to solve this issue: either fundamental conservation laws were broken in beta decays (Bohr) or a new, low interacting, neutral, negligible mass and spin 1/2 particle existed, which had yet to be detected (Pauli). The quest for detecting what we now know as the neutrino had started.

It took 26 years for the **first direct detection** to happen. It was thanks to Cowan and Reines who realized an inverse beta decay experiment and who would in 1995 receive the Physics Nobel prize for this discovery. They used reactor antineutrinos, which interacted with protons to produce a neutron and a positron [1]. The positron annihilated with an electron, generating two gamma rays while the neutron thermalized and then was captured by a cadmium atom dissolved in the detector water. This delayed pulse pair is an unique signature for the antineutrino, allowing for good background reduction.

2.1.1 Three neutrino flavours

Even before the direct detection of the first neutrino flavour by Cowan and Reines there were already suspicions of the **existence of additional flavours**. In 1948, muons were found to decay into electrons. The spectrum was continuous and matched with the emission of two undetected particles. However, at that time, there was no proof that both neutrinos were different.

In 1962, Lederman and Schwartz showed in the Brookhaven Laboratory that there existed more than one neutrino flavour after detecting the interactions of the muon neutrino, which earned them the 1988 Nobel Prize [3]. They generated a neutrino beam by in-flight decay of pions. The decay products were later seen in a spark chamber. Since only mesons were seen, and not electrons, those neutrinos had to be different to the ones in other experiments.

Strong hints of the **third neutrino flavour** were found on 1989 by the MARK-II collaboration at the SLC. Initial measurements of the $e^+e^- \to Z^0$ resonance gave an invisible width which matched with $3-5$ neutrino flavours [7], which was quickly narrowed down to 3 and excluding the fourth at 2σ [8]. Theoretical consistency considerations and more precise measurements later on by the LEP collaborations [65] made its existence clear. It was finally seen in Fermilab, by the DONUT collaboration in 2000 in a fixed target proton beam experiment [15]. For the same reasons that the tau neutrino was speculated, we also know that only three light active neutrino flavours exist. More recent measurements like cosmological bounds also point in the same direction [64].

2.1.2 Lepton number conservation & parity violation

Electron lepton number conservation was formulated by Zeldovich et al. in 1953. While the particle was assigned to be neutrino or antineutrino a priori to satisfy this conservation law, it wasn't known if they were the same particle or not. Two years later, Ray Davis would try to prove this by showing that antineutrinos from nuclear reactors couldn't trigger the conversion of chlorine into argon, for which neutrinos are required [17].

$$^{37}_{17}\mathrm{Cl} + \nu_e \to {}^{37}_{18}\mathrm{Ar} + e^- \tag{2.1}$$

The produced $^{37}_{18}$Ar is radioactive with a half life of 35 days. Since it's a gas, it can be siphoned out of the tank and its initial quantity ascertained by counting the number of radioactive decays. As there was no surplus of argon produced in his chlorine tanks near the Brookhaven Reactor versus the number of events measured far away at the same altitude, it was taken as a proof of the distinct nature of antineutrinos. However, with the discovery of parity violation in weak interactions, Davis' results could be explained as an helicity mismatch.

The $\theta - \tau$ puzzle was a very intriguing problem for particle physicists of the late 50's. Two different decays were found for these charged strange mesons:

$$\theta^+ \to \pi^+ + \pi^0 \qquad \tau^+ \to \pi^+ + \pi^+ + \pi^- \tag{2.2}$$

The intrinsic parity of a pion is -1 and since it's a multiplicative quantum number, both final states have different parities. With increasingly precise measurements, no difference was found between the masses and lifetimes of each, but for both initial states to be the same particle, **parity had to be broken** by weak interactions. After it was solved, both particles were seen to be the same, which we now call K^+.

Since little was known about strange particles, Lee and Yang didn't consider the $\theta - \tau$ puzzle sufficient evidence for P violation and thus proposed various experiments. The first was realized by **Wu**, following the process:

$$^{60}_{27}\mathrm{Co} \to {}^{60}_{28}\mathrm{Ni}^* + e^- + \bar{\nu}_e \to {}^{60}_{28}\mathrm{Ni} + e^- + \bar{\nu}_e + 2\gamma \tag{2.3}$$

The $^{60}_{27}$Co nuclei were aligned by a magnetic field, and by comparing the angular distributions of the e^- (emitted via weak interactions) to the γ (emitted via EM processes) anisotropies were found, confirming P violation. The second was conducted by **Goldhaber**, in which polarizations of gamma rays from β decays were measured. This was the first time neutrinos were proven to be left-handed.

2.2 Neutrino masses and oscillations

During the late 60s, Ray Davis carried out a new experiment, now in the Homestake gold mine. The same mechanism of converting chlorine into argon was used but now to measure the solar neutrino flux and validate Bahcall's SSM (Solar Standard Model, explained in 3.1). This time Davis' experiment was a success since the sun does emit neutrinos rather than antineutrinos, but the number of events was $\sim 1/3$ of the SSM prediction. Homestake continued running until 1994, measuring consistently the same deficit, and it was later confirmed by other experiments such as Kamiokande and GALLEX [34]. This was known as the **solar neutrino problem**.

Around that time, **Bruno Pontecorvo** had shown that if neutrinos had mass, a phenomenon in which they change from one flavour to another would occur. In that case, neutrino oscillations would be a lepton flavour violating process and they would explain the electron neutrino disappearance as a conversion into other flavours which went undetected in the chlorine tanks. While we now know that this is the case, other explanations were possible, like mid-flight decay of the neutrinos. Thus, Homestake's data wasn't enough, **the neutrino flux in non-electron flavours had to be measured** as well.

It would take a few decades and new, very precise measurements to solve the solar neutrino problem. In 2001, the SNO (Sudbury Neutrino Observatory) showed clear evidence of neutrino flavour change [16]. SNO was able to successfully tag solar neutrinos and also measure both neutrino fluxes via two different reactions in their deuterium tank:

$$\nu_e + d \to p + p + e^- \quad \text{(CC)} \qquad \nu_x + d \to p + n + \nu_x \quad \text{(NC)} \tag{2.4}$$

The CC (charged current, W boson exchange) interaction is sensible only to electron neutrinos while the NC (neutral current, Z boson exchange) is sensible to all of them. The ratio between both matched the predictions of massive neutrino oscillations.

Another discrepancy of similar nature happened with atmospheric neutrinos. The Kamiokande experiment, initially designed to measure proton decay, reported a ratio of muon neutrinos to electron neutrinos lower than expected (explained in 3.2). The **atmospheric neutrino anomaly** would be confirmed later by other experiments like IMB and Soudan-2. The cause of this neutrino anomaly would then be explained as $\nu_\mu \leftrightarrow \nu_\tau$ oscillations by Super Kamiokande [11], which granted **Takaaki Kajita** from Super Kamiokande together with Arthur McDonald from SNO the 2015 physics Nobel prize. Nowadays, even though each one of the individual neutrino masses haven't been measured, plenty of experimental evidence exists to support their oscillations.

2.2.1 PMNS matrix and oscillations in vacuum

The neutrino eigenstates of weak interaction (flavour, $|\nu_\alpha\rangle$ with $\alpha = \{e, \mu, \tau\}$) and hamiltonian (mass, $|\nu_i\rangle$ with $i = \{1, 2, 3\}$) don't have to necessarily match. That is, the rotation matrix U that relates both states doesn't have to be diagonal.

$$|\nu_\alpha\rangle = \sum_{i=1}^{3} U^*_{\alpha i} |\nu_i\rangle \tag{2.5}$$

This is indeed the case. The **rotation matrix** is known as the **PMNS** (Pontecorvo-Maki-Nakagawa-Sakata) matrix. In principle, this is a 3×3 unitary complex matrix, which amounts to $3^2 = 9$ real parameters, but five of them can be absorbed as phases of the lepton fields. Thus, it can be parametrized just by four real parameters, most

commonly three mixing angles (θ_{12}, θ_{23} and θ_{13}) and a CP-violating phase δ_{CP} [63].

$$\begin{aligned} U &= \begin{pmatrix} 1 & 0 & 0 \\ 0 & c_{23} & s_{23} \\ 0 & -s_{23} & c_{23} \end{pmatrix} \begin{pmatrix} c_{13} & 0 & s_{13}e^{-i\delta_{\text{CP}}} \\ 0 & 1 & 0 \\ -s_{13}e^{i\delta_{\text{CP}}} & 0 & c_{13} \end{pmatrix} \begin{pmatrix} c_{12} & s_{12} & 0 \\ -s_{12} & c_{12} & 0 \\ 0 & 0 & 1 \end{pmatrix} \\ &= \begin{pmatrix} c_{13}c_{12} & c_{13}s_{12} & s_{13}e^{-i\delta} \\ -c_{23}s_{12} - s_{23}s_{13}c_{12}e^{i\delta} & c_{23}c_{12} - s_{23}s_{13}s_{12}e^{i\delta} & s_{23}c_{13} \\ s_{23}s_{12} - c_{23}s_{13}c_{12}e^{i\delta} & -s_{23}c_{12} - c_{23}s_{13}s_{12}e^{i\delta} & c_{23}c_{13} \end{pmatrix} \end{aligned} \tag{2.6}$$

Where $c_{ij} = \cos\theta_{ij}$ and $s_{ij} = \sin\theta_{ij}$. Let us consider a neutrino produced in a weak interaction, and thus its initial state is a flavour eigenstate $|\nu_\alpha(0)\rangle \equiv |\nu_\alpha\rangle$, its state after some time t will be:

$$|\nu_\alpha(t)\rangle = \sum_{i=1}^{3} U^*_{\alpha i} |\nu_i(t)\rangle = \sum_{i=1}^{3} U^*_{\alpha i} e^{-iE_i t} |\nu_i\rangle \tag{2.7}$$

Since we will measure it via a weak interaction we have to rotate this into the flavour basis. Thus, the amplitude of oscillation from α to β will be:

$$\begin{aligned} A_{\nu_\alpha \to \nu_\beta}(t) &= \langle \nu_\beta | \nu_\alpha(t) \rangle = \sum_{i=1}^{3} U^*_{\alpha i} e^{-iE_i t} \langle \nu_\beta | \nu_i \rangle \\ &= \sum_{i,j=1}^{3} U^*_{\alpha i} U_{\beta j} e^{-iE_i t} \underbrace{\langle \nu_j | \nu_i \rangle}_{\delta_{ij}} = \sum_{i=1}^{3} U^*_{\alpha i} U_{\beta i} e^{-iE_i t} \end{aligned} \tag{2.8}$$

And the transition probability is just the amplitude squared

$$P_{\nu_\alpha \to \nu_\beta}(t) = \left| A_{\nu_\alpha \to \nu_\beta}(t) \right|^2 = \sum_{i,j=1}^{3} U^*_{\alpha i} U_{\beta i} U_{\alpha j} U^*_{\beta j} e^{-i(E_i - E_j)t} \tag{2.9}$$

Recall that $E_i = \sqrt{p^2 + m_i^2}$ and for relativistic neutrinos, $p \gg m_i$, thus

$$E_i = \sqrt{p^2 + m_i^2} \simeq p + \frac{m_i^2}{2p} \simeq p + \frac{m_i^2}{2E} \qquad \Longrightarrow \qquad E_i - E_j \simeq \frac{m_i^2 - m_j^2}{2E} \equiv \frac{\Delta m_{ij}^2}{2E} \tag{2.10}$$

In natural units, both distance and time have the same dimension. By using (2.10) and expressing (2.9) in terms of the distance traveled L we arive at:

$$P_{\nu_\alpha \to \nu_\beta}(L) = \sum_{i,j=1}^{3} U^*_{\alpha i} U_{\beta i} U_{\alpha j} U^*_{\beta j} \exp\left(-i \frac{\Delta m_{ij}^2 L}{2E} \right) \tag{2.11}$$

This equation condenses most of the key concepts in neutrino oscillations. For oscillations to occur, the corresponding matrix elements can't be zero and $\Delta m_{ij}^2 \neq 0$.

The oscillation probability is sinusoidal on L/E. In some cases, these dynamics can be reduced from 3 to 2 states as an approximation, which we study in the next chapter.

It is sometimes useful to further expand (2.11) into real and imaginary parts, since the physical effects of δ_{CP} will be isolated in the imaginary part (that is, $\delta_{\mathrm{CP}} = 0 \iff$ imaginary term $= 0$). Using $\cos x = 1 - 2\sin^2(x/2)$ we get:

$$\begin{aligned} P_{\nu_\alpha \to \nu_\beta}(L) = \delta_{\alpha\beta} - 4 \sum_{i>j} \mathrm{Re}\{U^*_{\alpha i} U_{\beta i} U_{\alpha j} U^*_{\beta j}\} \sin^2\left(\frac{\Delta m^2_{ij} L}{4E}\right) \\ +2 \sum_{i>j} \mathrm{Im}\{U^*_{\alpha i} U_{\beta i} U_{\alpha j} U^*_{\beta j}\} \sin\left(\frac{\Delta m^2_{ij} L}{2E}\right) \end{aligned} \tag{2.12}$$

In (2.6) we could multiply the Dirac PMNS matrix by a phase diagonal matrix

$$\begin{pmatrix} e^{i\alpha_1} & 0 & 0 \\ 0 & e^{i\alpha_2} & 0 \\ 0 & 0 & 1 \end{pmatrix} \tag{2.13}$$

where α_1 and α_2 are the Majorana phases. These phases can't be reabsorbed into the lepton fields but they vanish when computing oscillation probabilities.

2.2.2 Oscillations in matter - MSW effect

Neutrino oscillations in matter don't behave in the same way as in vacuum. This is known as the MSW (Mikheyev-Smirnov-Wolfenstein) effect. For a neutrino propagating in matter, the NC interaction is equal for all flavours which amounts to a common phase factor. However, **CC interactions introduce a flavour asymmetry** favouring electron neutrinos due to the high density of electrons in matter. Electron neutrino scattering in the forward direction is enhanced, in a similar way to forward scattering of light in a medium.

The effect of oscillations in matter is very important when interpreting neutrino oscillation results. For solar neutrinos one has to take into account both the propagation in vacuum and also the different propagation lengths inside the solar plasma. Since detectors, even those deep underground, are at first order on the surface of the Earth, there will be a difference in propagation lengths for upward and downward going neutrinos. For the case of atmospheric neutrinos, this was seen as early as 2004 [20] and for solar neutrinos, first evidences of terrestrial matter effects were seen 10 years later [35].

2.2.3 Mass hierarchy

As (2.11) shows, oscillation experiments let us measure the square mass splittings but not the individual masses. There are two non-equivalent mass orderings with this information, NO (normal order) with $m_1 < m_2 < m_3$ and IO (inverted ordering) with $m_3 < m_1 < m_2$. In addition to that, depending on the size of the masses with respect to the square mass splittings, they could be hierarchical or quasidegenerate. Based on current data, it's clear that **there is a certain hierarchy**. There is **some evidence favouring NO**: using just SK IV data, IO is disfavoured at 74% c.l. [62] and by combining SK I-IV + T2K, IO is disfavoured at more than 92% c.l. [53]. However, this is not conclusive and more data needs to be accumulated. Knowing which is the correct order is critical for many theories, as well as for the experimental determination of the other parameters.

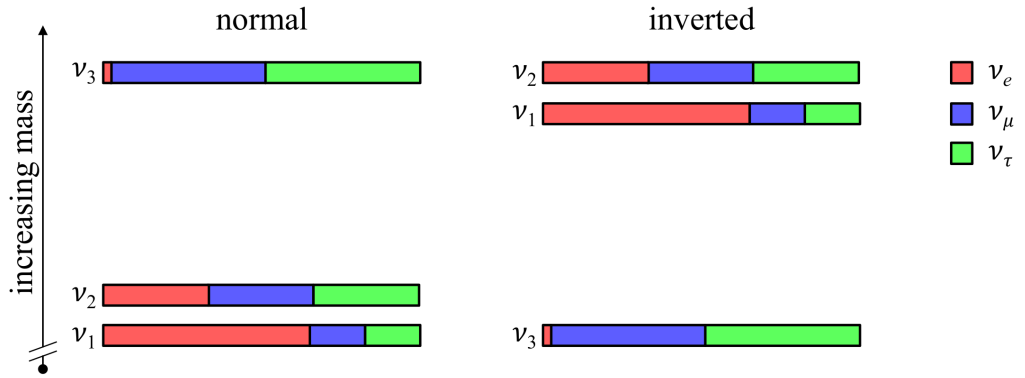

Figure 2.1: The two possible neutrino mass hierarchies. Colors represent the approximate flavour compositions of each mass eigenstate [44].

There are various ways of experimentally **determining the mass hierarchy** [44]:

- For neutrinos traveling through matter the enhancement of ν_e increases the effective masses of the ν_e-dominated states (ν_1 and ν_2), which either compresses or expands the effective mass splittings depending on the hierarchy, modifying the oscillation probabilities. This is the most important effect for the hierarchy determination in Super Kamiokande.

- Sufficiently precise measurements could show that if Δm^2_{31} is larger (smaller) than Δm^2_{32} then the hierarchy is normal (inverted).

- Cosmological measurements are sensible to the sum of neutrino masses. If this value is constrained enough such that it is lower than $\lesssim 2\sqrt{|\Delta m^2_{32}|} \sim 100$ meV, the hierarchy would have to be normal.

2.2.4 CP violation and parameter values

The topic of δ_{CP} is very interesting. It measures the symmetry breaking of the charge conjugation × parity. While **CPT must be a good symmetry** of any Lorentz invariant local QFT with hermitian hamiltonian, **CP doesn't have to**. Since CP violation is one of the Sakharov conditions, its breaking in the neutrino sector could provide an explanation to the problem of matter-antimatter asymmetry in the universe. From (2.11) one can compute the following probability: [60]

$$P_{\nu_\mu \to \nu_e} \approx \left\{ \sin^2(2\theta_{13}) \sin^2(\theta_{23}) \mp 8 J_{\text{CP},l} \frac{\Delta m^2_{21} L}{4E} \right\} \sin^2\left(\frac{\Delta m^2_{32} L}{4E} \right) \tag{2.14}$$

in which matter oscillation effects haven't been taken into account. The sign of the second term is − for neutrinos and + for antineutrinos and J_{CP} is the Jarlskog invariant, which encapsules the magnitude of the CP violation in that sector:

$$J_{\text{CP},l} = \frac{1}{8} \cos\theta_{13} \sin(2\theta_{12}) \sin(2\theta_{23}) \sin(2\theta_{13}) \sin(\delta_{\text{CP}}) \approx 0.033 \sin(\delta_{\text{CP}}) \tag{2.15}$$

For comparison, in the quark sector the Jarlskog invariant has been measured to be $J_{\text{CP},q} = 3 \times 10^{-5}$, so $J_{\text{CP},l}$ has the potential to be up to three orders of magnitude higher. In a long baseline accelerator experiment like T2K, this probability can be measured for both neutrinos and antineutrinos. Recent measurements from the T2K experiment, which uses Super Kamiokande as its far detector, have shown that **both non-CP violating angles** $\delta_{\text{CP}} = 0$ and $\delta_{\text{CP}} = \pi$ **are excluded** at 3σ and 2σ respectively. [60] This is the first time any δ_{CP} value has been excluded at 3σ. Gadolinium loading in Super Kamiokande allows for better sensitivity in discerning neutrinos from antineutrinos, which in turn can help in refining this measurement.

Table 2.1: Current values for the neutrino parameters. Mixing angles and mass splittings are obtained as a global analysis of multiple colaborations, including SK atmospheric data [57]. The published version includes data up to fall 2018, while the online (`www.nu-fit.org`) is updated to July 2019, which is what we show here. Δm^2_{3l} is Δm^2_{31} for NO and Δm^2_{32} for IO. For δ_{CP}, the more recent T2K+SK value is shown [60].

	Normal Ordering		**Inverted Ordering**	
	$\pm 1\sigma$ range	**$\pm 3\sigma$ range**	**$\pm 1\sigma$ range**	**$\pm 3\sigma$ range**
$\boldsymbol{\sin^2\theta_{12}}$	$0.310^{+0.013}_{-0.012}$	$0.275 \to 0.350$	$0.310^{+0.013}_{-0.012}$	$0.275 \to 0.350$
$\boldsymbol{\sin^2\theta_{23}}$	$0.563^{+0.018}_{-0.024}$	$0.433 \to 0.609$	$0.565^{+0.017}_{-0.022}$	$0.436 \to 0.610$
$\boldsymbol{\sin^2\theta_{13}}$	$0.02237^{+0.00066}_{-0.00065}$	$0.02044 \to 0.02435$	$0.02259^{+0.00065}_{-0.00065}$	$0.02064 \to 0.02457$
$\boldsymbol{\delta_{\text{CP}}/\text{rad}}$	$-1.89^{+0.70}_{-0.58}$	$-3.41 \to -0.03$	$-1.38^{+0.48}_{-0.54}$	$-2.54 \to -0.32$
$\boldsymbol{\Delta m^2_{21}/10^{-5}\text{eV}^2}$	$7.39^{+0.21}_{-0.20}$	$6.79 \to 8.01$	$7.39^{+0.21}_{-0.20}$	$6.79 \to 8.01$
$\boldsymbol{\Delta m^2_{3l}/10^{-3}\text{eV}^2}$	$2.528^{+0.029}_{-0.031}$	$2.436 \to 2.618$	$-2.510^{+0.030}_{-0.031}$	$-2.601 \to -2.419$

Many experiments are dedicated to finding the precise values of the angles and mass splittings, Super Kamiokande among them. In (Table 2.1) their values for both NO and IO are shown from a global analysis which merges data from multiple experiments. A discussion about the parameters and which experiments are more precise at measuring each of them is realized in the next chapter.

Aside from the square mass splittings we can know bounds for the sum of the masses of the three light neutrino flavours $m_{\text{tot}} \equiv \sum_{i=1}^{3} m_{\nu_i}$. From a cocktail of cosmological measurements[1] an upper bound can be obtained [56] and based on oscillation experiments, a lower bound [22], resulting in the following mass range:

$$60 \text{ meV} < m_{\text{tot}} < 118 \text{ meV} \tag{2.16}$$

2.2.5 Could there be one massless neutrino?

While it isn't ruled out by the experiment, the lightest neutrino mass state being massless is **highly improbable**. For its mass to be exactly zero, an unknown symmetry would have to protect it. In addition to that, in that massless field it would be possible to reabsorb the CP violating phase as a global phase (like in Peccei-Quinn mechanism) and thus there would be no measurable CP violation for that field. The recent δ_{CP} measurements are the best way to rule out this massless neutrino without getting into symmetry speculations.

2.3 Neutrino mass generation

In the SM (Standard Model), mass terms for particles such as W/Z bosons, leptons and quarks can't be directly included in the lagrangian since they wouldn't be both renormalizable and gauge invariant. After the experimental discovery of the Higgs boson in 2012, the Brout-Englert-Higgs mechanism as a way of giving particles mass in the SM was consolidated. However, since neutrinos are only left-handed and we need to couple them to another right-handed fermion to be able to build a mass term via the Higgs mechanism, **SM neutrino masses are precisely zero**.

Although the number of active light neutrino flavours is heavily constrained by experiments, we can still add an arbitrary number of **sterile neutrinos** to the theory, which don't have weak charge. These could potentially be measured in oscillation experiments in case that the data can't be fitted with only three flavours, as sterile neutrinos would participate in oscillations just like the active flavours. After including sterile neutrinos we can form both Dirac and Majorana mass terms.

As of today, the **Dirac vs Majorana** nature of neutrinos hasn't been settled. Neutrinoless double beta decay experiments are very promising since the matrix element of the process depends on the difference of majorana phases.

[1] 2015 Planck CMB temperature + 2016 Planck reionization optical depth + BOSS BAO + MGS + 6dFGS + Pantheon SN type Ia + high-l CMB polarization data.

Chapter 3

Neutrino sources and experiments

We know about a plethora of different neutrino sources (Figure 3.1). Each of them has its peculiarities, allowing us to study with better precision different neutrino parameters (Table 3.1), different square mass splittings (Table 3.2) as well as to check various astrophysical and cosmological models. In this chapter we will do a review of most of the processes that generate neutrinos in nature, as well as the different experimental techniques developed. Special emphasis has been given to the sources most relevant to the Super Kamiokande and SuperK-Gd experiments.

Table 3.1: Experiments contributing to the present determination of the values of the various oscillation parameters [63].

Experiment type	**Notable examples**	**Dominant**	**Important**
Solar experiments	*SNO, SK, borexino*	θ_{12}	$\Delta m^2_{21}, \theta_{13}$
Reactor LBL	*KamLAND*	Δm^2_{21}	θ_{12}, θ_{13}
Reactor MBL	*Daya-Bay, Reno, D-Chooz*	$\theta_{13}, \left\|\Delta m^2_{31,32}\right\|$	
Atmospheric exp.	*SK, IC-DC*	$\theta_{23}, \left\|\Delta m^2_{31,32}\right\|$	$\theta_{13}, \delta_{\mathrm{CP}}$
Accel. LBL ν_μ, $\bar{\nu}_\mu$ disapp.	*K2K, MINOS, T2K, NOνA*	$\left\|\Delta m^2_{31,32}\right\|, \theta_{23}$	
Accel. LBL ν_e, $\bar{\nu}_e$ app.	*MINOS, T2K, NOνA*	$\delta_{\mathrm{CP}}, \theta_{13}$	θ_{23}

Table 3.2: Characteristic values of neutrino propagation length L and neutrino energy E for various sources and experiments as well as the square mass splitting Δm^2 ranges to which they can be the most sensitive, as seen from (2.11). [23]

Experiment		**L(m)**	**E(MeV)**	$\boldsymbol{\Delta m^2(\mathrm{eV}^2)}$
Solar		10^{10}	$1-10$	10^{-10}
Atmospheric		$10^4 - 10^7$	$10^2 - 10^5$	$10^{-1} - 10^{-4}$
Reactor	SBL	$10^2 - 10^3$	$1-10$	$10^{-2} - 10^{-3}$
	LBL	$10^4 - 10^5$		$10^{-4} - 10^{-5}$
Accelerator	SBL	10^2	$10^3 - 10^4$	> 0.1
	LBL	$10^5 - 10^6$	10^4	$10^{-2} - 10^{-3}$

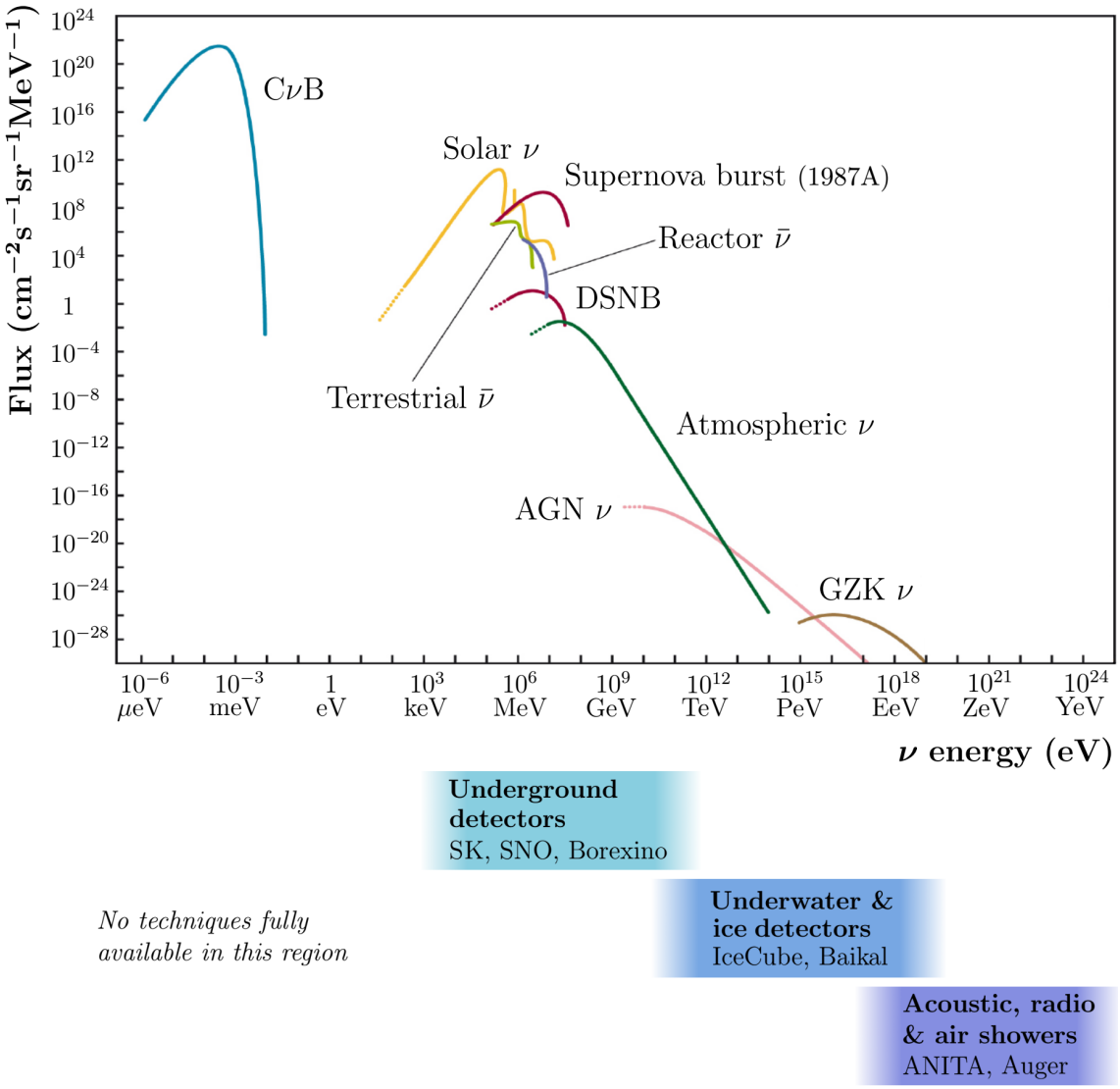

Figure 3.1: Neutrino fluxes as a function of energy for most sources as well as the energy ranges searched by different experiments. From the least energetic: CνB (cosmic neutrino background), solar ν, terrestrial and reactor $\bar{\nu}$, supernova bursts and DSNB (diffuse supernova neutrino background), atmospheric ν, AGN ν (active galactic nuclei) and finally GZK ν (Greisen-Katsepin-Kuzmin, cosmogenic). Adapted and expanded from [27].

3.1 Solar neutrinos

The **SSM** (standard solar model) by John Bahcall states that stars generate their energy through nuclear fusion in two different ways, the CNO (carbon-nitrogen-oxygen) cycle and the pp (proton-proton) chain. For a star the size of the Sun, the pp chain accounts for $\sim 98.4\%$ of its total luminosity. In this chain, five different reactions produce neutrinos. Neutrinos from pep and ^{7}Be are monochromatic while the rest are emitted in a continuous spectrum up to a maximum energy.

Table 3.3: The 5 processes in the pp chain and the corresponding ν energy ranges [6].

[pp]	$p + p \rightarrow {}^2\mathrm{H} + e^+ + \nu_e$	< 0.42 MeV
[pep]	$p + e^- + p \rightarrow {}^2\mathrm{H} + \nu_e$	1.442 MeV
[^{7}Be]	${}^7\mathrm{Be} + e^- \rightarrow {}^7\mathrm{Li} + \nu_e$	$0.861, 0.383$ MeV
[^{8}B]	${}^8\mathrm{B} \rightarrow {}^8\mathrm{Be}^* + e^+ + \nu_e$	< 14.06 MeV
[hep]	${}^3\mathrm{He} + p \rightarrow \alpha + e^+ + \nu_e$	< 18.77 MeV

Different detection techniques have each their own peculiarities [23].

- **Chlorine** radiochemical experiments like Homestake were the first to measure solar neutrinos, which are captured via the CC ${}^{37}_{17}\mathrm{Cl} + \nu_e \rightarrow {}^{37}_{18}\mathrm{Ar} + e^-$ reaction with a $E_\nu > 0.814$ MeV energy threshold.

- **Gallium** radiochemical experiments were designed as successors of chlorine, employing the CC ${}^{71}_{31}\mathrm{Ga} + \nu_e \rightarrow {}^{71}_{32}\mathrm{Ge} + e^-$ reaction. Properties of this target include a lower energy threshold of $E_\nu > 0.233$ MeV and a stronger transition, thus larger cross section for the lower energy ν. Notable experiments are SAGE, GALLEX and its sucessor GNO.

- **Water Cherenkov** experiments detect the electrons emitted from the water by ES (elastic scattering) $\nu + e^- \rightarrow \nu + e^-$. Scattered electrons travel faster than the speed of light in the dielectric medium, which gets polarized and in turn emits Cherenkov light, which is then detected by the PMTs (photomultipliers) in the walls. Unlike radiochemical experiments, elastic scattering experiments are sensible to all neutrino flavours, but favour ν_e since they are the only ones that undergo CC interactions. Notable experiments are Kamiokande ($E_\nu > 7.5$ MeV) and its sucessor Super Kamiokande ($E_\nu > 4$ MeV).

- **Deuterium Cherenkov** detectors like SNO measure energetic neutrinos via three different reactions: CC for electron neutrinos with $E_\nu > 5$ MeV, NC for all active neutrinos with $E_\nu > 2.225$ MeV and ES also for all flavours, but with a smaller cross section. For solving the solar neutrino problem, SNO used ^{8}B neutrinos since they're the only ones abundant enough above their threshold. Both water and deuterium Cherenkov experiments allow for measurement of time, direction and energy of the neutrino, unlike radiochemical experiments.

- **Liquid scintillator** experiments like Borexino are designed to measure the lowest energy solar neutrinos in real time. It detects them via elastic scattering, again favouring electron neutrinos.

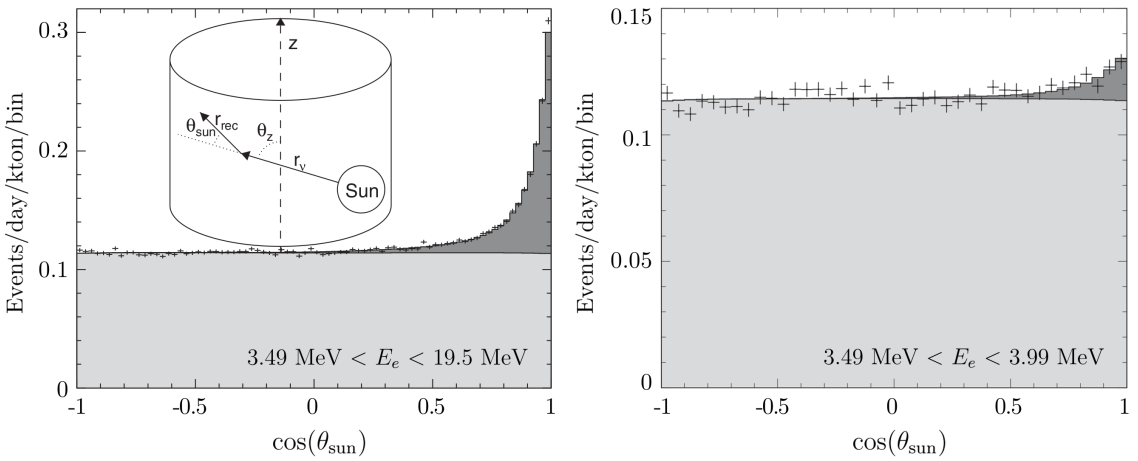

Figure 3.2: Solar angle distributions for electron energies of $3.49 - 19.5$ *MeV (left) and* $3.49 - 3.99$ *MeV (right). The dark (light) shaded region is the solar neutrino signal (background) component [45].*

For the measurement of low energy solar ν, Gd loading will have a negative impact. As we can see in (Figure 3.2), for the full energy range the signal to background ratio is big but once we restrict the histogram only to low energy ν, an increase of the background would most probably hinder this measurement.

So far the only solar neutrinos which haven't been detected are the ones from the **hep** reaction. The strongest claims come from SNO [49] which exclude no hep flux at 2σ. The future experiments DUNE and HK have the potential sensibility to measure them with greater precision (Fig. 4 [55] and Fig. 160-161 [54] respectively). The first measurement of the **CNO neutrinos** at 5σ by Borexino was just shown at the Neutrino 2020 conference [70].

3.1.1 Solar regime

The probability of an electron neutrino not oscillating would be, following (2.12):

$$\begin{aligned} P_{\nu_e \to \nu_e}(L) &= 1 - 4U_{e2}^2 U_{e1}^2 \sin^2\left(\frac{\Delta m_{21}^2 L}{4E}\right) = 1 - 4c_{13}^2 s_{12}^2 c_{13}^2 c_{12}^2 \sin^2\left(\frac{\Delta m_{21}^2 L}{4E}\right) \\ &= 1 - \cos^4\theta_{13} \sin^2 2\theta_{12} \sin^2\left(\frac{\Delta m_{21}^2 L}{4E}\right) \simeq 1 - \sin^2 2\theta_{12} \sin^2\left(\frac{\Delta m_{21}^2 L}{4E}\right) \end{aligned} \tag{3.1}$$

The last step follows from taking $\theta_{13} \approx 0$. As we know from (Table 2.1), θ_{13} is the smallest angle and in this case it plays a subleading role. Confirming what was shown in (Table 3.1), solar experiments are mostly sensible to θ_{12}

As we can see from (3.1), there is a dependence on Δm_{12}^2 so solar experiments can measure that parameter. However, the long propagation length together with low neutrino energies make solar experiments best at measuring splittings near 10^{-10} eV^2 (Table 3.2).

3.2 Atmospheric neutrinos

Cosmic rays are extremely energetic particles, mostly protons but may also be other nuclei. Upon impact with the particles in Earth's atmosphere they create hadronic showers. Amongst the newly generated particles there are many charged pions, which decay producing neutrinos in the process.

$$\begin{aligned} \pi^+ &\to \mu^+ + \nu_\mu \to e^+ + \nu_e + \bar{\nu}_\mu + \nu_\mu \\ \pi^- &\to \mu^- + \bar{\nu}_\mu \to e^- + \bar{\nu}_e + \nu_\mu + \bar{\nu}_\mu \end{aligned} \tag{3.2}$$

Both kinds of charged pions will be generated in similar amounts, so in this simplified model the expected ratio of muon to electron neutrinos and antineutrinos is:

$$R = \frac{\nu_\mu + \bar{\nu}_\mu}{\nu_e + \bar{\nu}_e} \sim 2 \tag{3.3}$$

This is true mostly for neutrinos of energies < 1 GeV [34], since for high energy cosmic rays some of the muons may reach the surface before decaying, increasing the ratio R. Collaborations like Super Kamiokande use Monte Carlo simulations for the precise calculation of the neutrino fluxes. While individually there's a 20% error for the simulated flux of each flavour, their ratios are more precise (5%), which is the reason atmospheric results are often given in terms of ratios.

Kamiokande reported an atmospheric neutrino deficit of $R_{\text{data}}/R_{\text{MC}} \sim 60\%$ in 1992 [9]. This deficit had a strong zenith angle and energy dependence, pointing towards travel distance dependent oscillation/decay effects. The solution, as we now know, is **$\nu_\mu \leftrightarrow \nu_\tau$ oscillations**. Kamiokande was able to observe the first evidences of these oscillations in 1998 [11] and Super Kamiokande measured the dip corresponding to the first maximum of oscillation probabilities in 2004 [20].

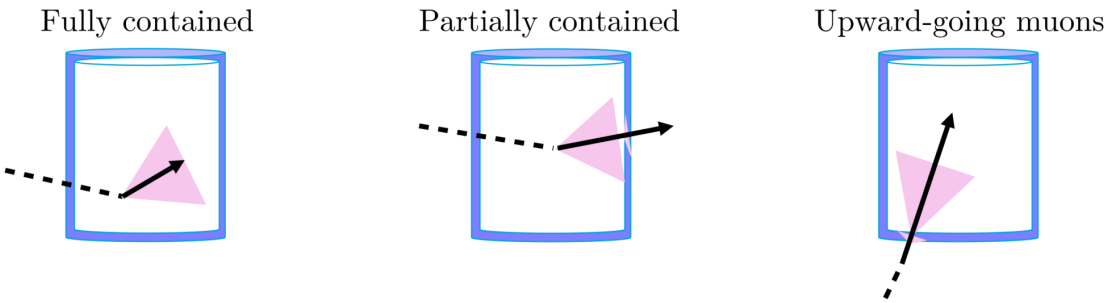

Figure 3.3: Most relevant event types in water Cherenkov experiments.

Neutrinos can be detected in underground water Cherenkov experiments by direct observation of a CC interaction inside the detector, in which case it is called a contained event. Depending if the charged lepton escapes or remains inside the detector volume they're called **partially** and **fully contained events** respectively. These last ones are best for the determination of flavour, kinetic energy and direction.

If the CC interaction happened outside the detector, some ν_μ can still be observed and they're **called upgoing muons**. Downgoing muons can't be distinguished from the cosmic ray background.

In water Cherenkov detectors, electron and muon events can be distinguished by the shape of the light emitted by their respective charged leptons. ***e*-like** events have diffuse rings since some of their energy is emitted in bremsstrahlung and other processes while ***μ*-like** events have more sharp light rings, as those are purely Cherenkov. Some example events can be seen in (Figure 3.4).

The experiment uses tagging programs to distinguish neutrino-like events from cosmic muons and also to distinguish each event type. When the Super Kamiokande detector is working, randomly chosen real time events can be seen on the online Super Kamiokande real time monitor[1], which is used by SK members as a quick way to check that the detector is working correctly. One must note that most of the events shown there are cosmic muons, characterized for being very bright and leaving a signal on the outer detector, which neutrino events don't.

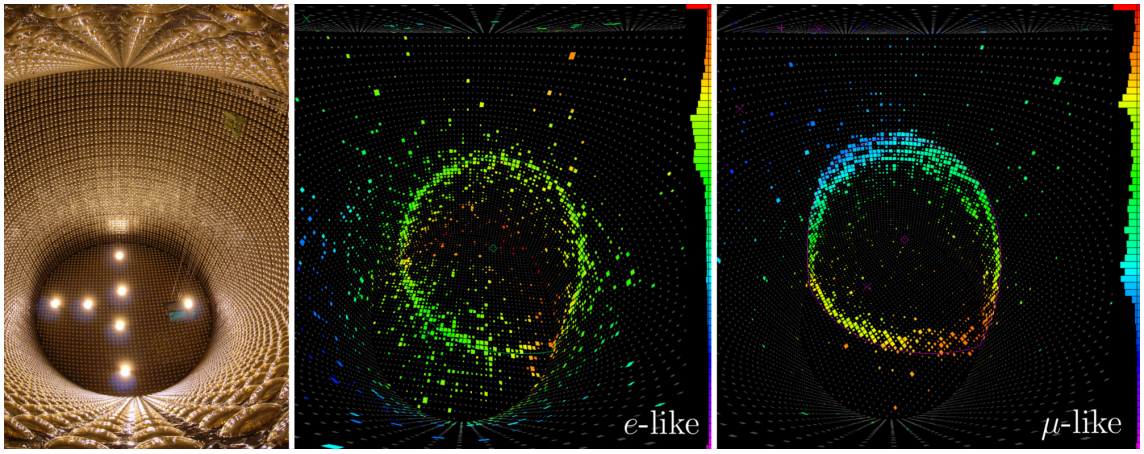

Figure 3.4: Neutrino event candidates in Super Kamiokande. From left to right: The SK inner detector, an e-like event, a μ-like event. The colour of each point indicates the time each signal arrived to the PMTs, purple being earlier and red later [37].

3.2.1 Atmospheric regime

We can better understand atmospheric neutrino oscillations by again doing some approximations in (2.12). In this case, not only θ_{13} is small but also L/E, thus allowing us to neglect $\Delta m^2_{12} L/E \sim 0$. In that case, $\Delta m^2_{31} = \Delta m^2_{21} + \Delta m^2_{32} \sim \Delta m^2_{32}$. Again, θ_{13} is small, which allows us to simplify the PMNS matrix to the following:

$$U \simeq \begin{pmatrix} c_{12} & s_{12} & 0 \\ -c_{23}s_{12} & c_{23}c_{12} & s_{23} \\ s_{23}s_{12} & -s_{23}c_{12} & c_{23} \end{pmatrix} \tag{3.4}$$

[1] `http://www-sk.icrr.u-tokyo.ac.jp/realtimemonitor/`

The e and μ oscillation probabilities can be calculated to be:

$$P_{\nu_e \to \nu_e} = 1 \qquad P_{\nu_e \to \nu_\mu} = 0 \qquad P_{\nu_\mu \to \nu_e} = 0 \tag{3.5}$$

$$\begin{aligned} P_{\nu_\mu \to \nu_\mu}(L) &= 1 - 4U_{\mu 3}^2 \left(U_{\mu 1}^2 + U_{\mu 2}^2\right) \sin^2\left(\frac{\Delta m_{23}^2 L}{4E}\right) \\ &= 1 - 4s_{23}^2 \left(c_{23}^2 c_{12}^2 + c_{23}^2 s_{12}^2\right) \sin^2\left(\frac{\Delta m_{23}^2 L}{4E}\right) \\ &= 1 - \sin^2(2\theta_{23}) \sin^2\left(\frac{\Delta m_{23}^2 L}{4E}\right) \end{aligned} \tag{3.6}$$

From this we know that in atmospheric oscillations, mainly $\nu_\mu \leftrightarrow \nu_\tau$ oscillations happen and the relevant parameters are θ_{23} and Δm_{23}^2. We can also see that maximal mixing occurs when $\theta_{23} = \pi/4$, which is near the observed value for this parameter.

Atmospheric neutrino measurements are also important for the determination of δ_{CP} and the mass hierarchy, although that can't be seen from this calculation. Due to the aforementioned matter effects, there will be a hierarchy-dependent upward-going excess of either electron neutrinos or antineutrinos. The angle δ_{CP} has some high order modulation effects on the oscillations but the differences in the oscillations of ν and $\bar{\nu}$ is the most important effect [53]. Distinguishing neutrinos from antineutrinos is vital in both cases, so here Gd doping is incredibly useful.

3.3 Reactor antineutrinos

Nuclear power plants produce high quantities of $\bar{\nu}_e$ from the beta decay of heavy particles in the various fission chains.

Dedicated reactor experiments can utilize those neutrinos for physics purposes. This experiments are typically Gd-doped **liquid scintillator** experiments, like Daya-Bay in China, RENO in Korea or Double Chooz in France. As we explain later in (Chapter 4), dissolving gadolinium in your detector volume maximizes the neutron capture efficiency, creating a delayed pulse pair signature which allows for good background reduction. It follows the same reasoning of the use of cadmium in Cowan and Reines experiment, but more efficient. Multiple detectors are often used to reduce the errors in nuclear reactor flux predictions, like Daya-Bay and RENO which have six of them. Double Chooz takes a different approach by having only one far and one near detector and taking data from two close nuclear plants.

There are various kinds of reactor experiments, **LBL** (long baseline), **MBL** (medium baseline) and **SBL** (short baseline), depending on the neutrino propagation length. This length has to be tuned to match the expected oscillation maximum, thus each type being more sensible to different mass splitting ranges (Table 3.2).

If a water Cherenkov detector is surounded by enough sufficiently close nuclear power plants, reactor neutrinos can be seen in the same energy range as solar neutrinos. Nuclear reactors usually have the same energy output during the day than during the night while there is a day-night asymmetry in solar neutrinos, so reactor antineutrinos are seen as one of the components of the constant background in those measurements (Figure 3.2). With Gd doping, they could be distinguished, allowing for both datasets to be separated which is both background reduction and also an increase in the precision of the measurement. SuperK-Gd is expected to have a sensibility to reactor antineutrinos higher than KamLAND but smaller than the best dedicated reactor experiments.

3.4 Accelerator neutrinos

Accelerator experiments operate under the same logic of atmospheric neutrinos, but on a more controlled manner. Proton beams collide into a fixed target, producing charged pions and kaons. Since those particles are charged, they can be focused with magnets so when they decay to neutrinos those are generated in a **beam**. The composition and energy of the neutrino beam can be further determined by selecting the sign of the pions and stopping the produced muons [23]. Just like reactor experiments, these are classified depending on the baseline length.

Especially relevant to this thesis is the **T2K** (Tokai to Kamioka) experiment. It is the successor of the K2K experiment and its neutrino beam is directed towards the Super Kamiokande detector, slightly off-axis (2.5 degrees) since that allows for maximal oscillation probability at the 295 km baseline length for 600 MeV neutrinos. The off-axis configuration also reduces the amount of high energy neutrinos in the beam, which for this experiments are mostly background events. Aside from SK as its far detector, it has various near detectors for measuring the neutrino flux before the oscillations.

LBL accelerator experiments are extremely precise ways of determining the θ_{23} angle, as well as the CP violating phase. While there are short baseline accelerator experiments, their achievements aren't as notorious as the ones from LBL.

3.5 Neutrino astronomy

Neutrino astronomy is a unique tool in development for understanding many questions in astrophysics, like refining supernova models, the origins of the most energetic cosmic rays and gamma rays, new unseen neutrino sources... its great potential −in a similar way to gravitational waves− comes from the small interaction cross section with matter which allows them to travel unaltered through regions opaque to light.

3.5.1 Supernova bursts

Although supernovae are rare within our galaxy, they're sufficiently bright to be optically seen in distant ones. They are classified according to their spectra in two main categories: **Type I**, which lack hydrogen absorption lines in their spectrum and **Type II**, which do have them. Further spectral classifications exist: Type Ia (which have a Si line at 615 nm) occur due to **thermal runaway**, in which material is accreted from a companion star, raising its core temperature enough to trigger carbon fusion. This supernova are very useful in astronomy for distance measurements. However, since most of the energy is directed into heavy element synthesis and the kinetic energy of ejected material, they aren't expected to produce a significant number of neutrinos [29].

All other spectral types (Type Ib/c & Type II-P/-L/n/b) happen due to **core collapse**. This happens when nuclear fusion becomes unable to sustain the core against its own gravity. The initial collapse is accelerated by beta decay ($n \rightarrow p + e^- + \bar{\nu}_e$), photodisintegration ($X + \gamma \rightarrow X^* \rightarrow Y + n/p/\alpha$) and electron capture ($p + e^- \rightarrow n + \nu_e$). Neutrinos from these processes are called **Si-burning phase neutrinos**. Some hours to days later, neutrino-antineutrino pairs of all flavours are produced by **thermal emission**, which are several orders of magnitude more abundand than those from the former processes. This results in a neutrino burst of ~ 10 seconds emitted hours before the peak of the supernova light emission.

Kamiokande was able to observe the first and, to date, only supernova event with neutrinos [5]. It was the type II supernova **1987A**, from the Large Magellanic Cloud, a dwarf satellite galaxy 50 kpc away from the Milky Way. Twelve neutrinos were detected, which arrived 3 hours before the supernova photons. Neutrino bursts further away than this one are almost impossible to detect with current technology. The closest galaxy, Andromeda, is ~ 770 kpc away from the Milky way. The neutrino flux decreases with the distance squared and for events this far, only one or zero neutrinos are expected to interact in the detector.

No supernova in the Milky Way has been observed since the invention of the optical telescope, so neutrino detectors are one of the most valuable tools not to miss the next event. Collaborative efforts like **SNEWS** (SuperNova Early Warning System) have been established for the early alert of this rare phenomena. As of today, seven experiments (Borexino, Daya Bay, KamLAND, HALO, IceCube, LVD, and Super Kamiokande) form this collaboration [19].

Since experiments like Super Kamiokande can point the direction of the supernova up to a few degrees of accuracy, that allows observatories to know where to look. Supernova neutrino flux also sheds light on the inner workings of the supernova, much more than its electromagnetic counterpart, allowing for refinement of the astrophysical models.

3.5.2 Diffuse Supernova Neutrino Background

As we have seen, neutrinos from single supernova events from outside of the Milky Way are virtually impossible to be measured with current technology. However, the integrated flux could be measured. This is called DSNB (Diffuse Supernova Neutrino Background) and is expected to be a weak and mostly isotropic, time-independent source of MeV neutrinos and antineutrinos from distant core-collapse supernovae. While it hasn't been detected yet, the SK upper limits are close to predictions, so it is expected that with Gd-doping the background will be reduced and energy range increased, allowing for a DSNB detection of a few events per year [26].

3.5.3 Relic neutrinos from primordial black holes

After Hawking described the quantum evaporation of black holes, it was suggested that black holes in the early Universe could evaporate to standard model particles. This has yet to be detected. The most astringent bounds are obtained from the absence of 100 MeV photons. For neutrinos, they are expected on the MeV range at a flux around $\sim 10^3$ times lower than atmospheric neutrinos [10]. Once the DSNB flux is measured, if the corresponding supernova rate doesn't match with the one obtained from optical measurements, it could be an indication of the existence of this kind of neutrinos.

3.5.4 Other sources

There are other sources for neutrino astronomy like the **cosmic neutrino background**, which is in an energy range so low that no experimental techniques have been developed enough for its measurement.

Neutrinos of energies of **TeV and beyond** are also important since their flux is related to the cosmic ray flux. Multiple experimental techniques exist (Underwater & under-ice neutrino telescopes, air shower detection, radio & acoustic techniques). IceCube and ANITA are two notable experiments in this energy range. None of the neutrinos from these sources can be seen in Super Kamiokande.

Chapter 4

The SuperK-Gd project

Located near the Kamioka mine, on the border between Toyama and Gifu prefectures in Japan, the Kamioka Observatory has been one of the most important places in the history of physics, as two Nobel prizes have been awarded to the research conducted in the observatory. It has been home to the Kamiokande experiment and more recently of KAGRA (for gravitational waves), KamLAND (for reactor $\bar{\nu}$), XMASS and NEWAGE (both for dark matter) and of course the four phases of the Super Kamiokande, as well as the future Hyper Kamiokande.

The Kamiokande experiment was originally named after its location and purpose: *Kamioka Nucleon Decay Experiment*. After the observation of the 1987A supernova [5] it was coloquially referred to as *Kamioka Neutrino Detection Experiment*, which conveniently has the same acronym. The Super Kamiokande experiment was built as its sucessor and while it still serves its purpose as a nucleon decay experiment, measuring neutrino oscillations is the main focus of the project. The Kamioka Observatory and Super Kamiokande are operated and owned by the Tokyo's Institute for Cosmic Ray Research (ICRR). There are over 150 SK collaborators and more than 40 institutions from Japan, the United States, Korea, China, Poland, Spain, Canada, UK, Italy and France.

Various **phases** of the project have already taken place. SK began taking data in April 1996 and was shut down for maintenance in July 2001, which constitutes its first phase (SK-I). While refilling the water tank, and accident occurred in which more than half of the PMTs were destroyed. It was rebuilt with half the original PMT density until it was completely rebuilt in July 2006. In September 2008 the most recent phase started, SK-IV, which new front-end electronics. In late 2018, after some tank refurbishments, SK-V commenced. The initial phase of the SuperK-Gd project is starting now, in which the first 14 tons of gadolinium salt will be dissolved to allow for a neutron tagging efficiency of about 50%. After careful analysis of the detector performance, the loading of the following 85 tons for 90% efficiency will hopefully be completed during the next two years.

4.1 The Super Kamiokande experiment

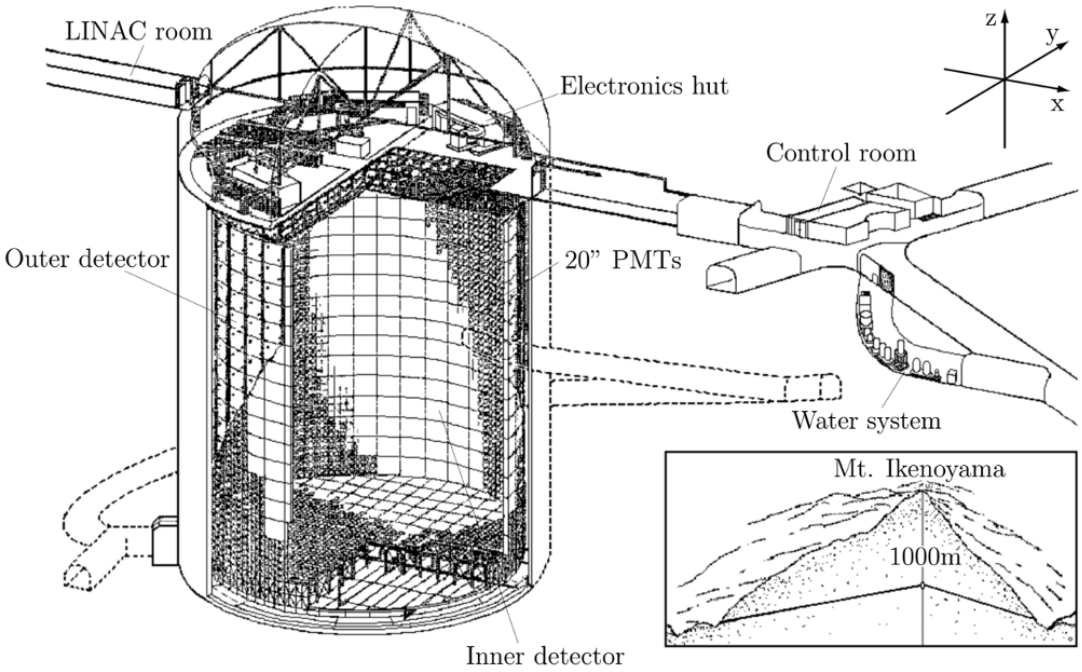

Figure 4.1: Scheme and location of the Super Kamiokande detector [51].

Since Super Kamiokande is the precursor and base experiment for SuperK-Gd, it is important to know in detail how it works. It is mainly a neutrino detector for astrophysical, solar and atmospheric neutrinos, as well as the far detector for the T2K beam. It is the current leader in nucleon decay bounds (Figure 4.7) and it can even be used for some dark matter searches.

The detector is comprised of a cylindrical tank, 39.3 m in diameter and 41.4 m in height, filled with 50 kton of ultrapure water. It was built with a 1000m of rock overburden, equivalent to setting the experiment 2700 m underwater [51], which causes a reduction of the cosmic ray muon background by around 5 orders of magnitude. The water tank is split into an outer and inner detector (OD & ID), which are concentric cylinders.

The **OD** extends $\sim$2 m out from the ID and is covered in 1885 outward facing 8-inch diameter PMTs. Since the OD is used as a veto for incoming cosmic ray muons, this low photocoverage is acceptable. A $40 - 50$ cm layer of reinforced concrete surounds the cavity and the are is covered in a polyurethane material called *Mineguard*, both serving the function of shielding the detector and its workers from radioactive emanations of the rock. A large dome above the tank is used to store the data acquisition electronics, calibration equipment and other related materials.

The **ID** consists of 32 kton of water, but its fiducial volume (the volume in which background events are largely excluded) is just 22.5 kton, 2 m away from the ID wall. This is due to the radioactive activity of the PMTs and other electronics.

It is surrounded by 11146 inward facing 20-inch diameter PMTs evenly distributed, allowing for around 40% photocoverage. A supporting frame separates both ID and OD, housing all the PMTs, covered in a black polyethylene terephtalate sheet to prevent light leaks between the two regions.

A photomultiplier tube (**PMT**) is a vacuum tube specialized in the precise detection of light. When photons enter through the input window, they can excite electrons in the photocatode through photoelectric process with a probability defined as quantum efficiency, which depends on the PMT construction and the photon energy. These electrons are acccelerated, focused and multiplied several times until they are finally collected and measured. The ID PMTs are sensitive to wavelengths in a range $300-600$ nm, with a quantum efficiency peak on ~ 400 nm of around 21%. This is calibrated to match the wavelength of the expected Cherenkov radiation.

Since PMTs use magnetic fields for the electron multiplication process, they are affected by Earth's geomagnetic field. 26 Helmholtz coils are set up around the walls of the tank to reduce this field by a factor of ten [18].

4.1.1 Cherenkov emission

In a dielectric material like water, the effective speed of light in that material gets reduced by a factor of $1/n$, where n is the refractive index of the medium. When a charged particle passes through a dielectric at a speed $\beta > 1/n$ ($\beta \equiv v/c$), it emits a light cone in the original direction of the particle motion. This emission is due to an asymmetric polarization of the medium in front and rear of the particle, giving rise to a varying electric dipole moment.

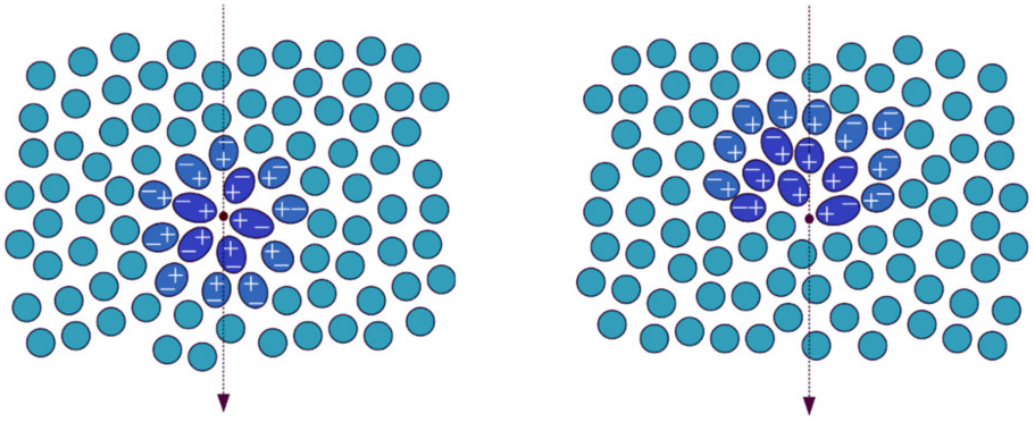

Figure 4.2: Simplified picture of the polarization configurations during the propagation of a charged particle in a dielectric. Left, $\beta < 1/n$, right, $\beta > 1/n$.

Some of the particle energy is converted into light and a coherent wavefront is generated at a certain angle θ_c which follows from the equation:

$$\cos(\theta_c) = \frac{1}{n\beta} = \frac{1}{n}\sqrt{1 - \frac{m}{|\vec{p}|}} \tag{4.1}$$

Where m is the particle mass and $\vec{p}$ its momentum. For ultrapure water, $n = 1.33$ and particles travel at speeds close to c, thus $\beta \simeq 1$. For this values, the typical Cherenkov angle is $\theta_c = \text{acos}(1/1.33) \simeq 41.2°$. The spectra can be calculated with the Frank–Tamm formula and is maximal at 375 nm, which is blue light. This explains the usual blue glow seen in nuclear reactors.

4.1.2 Water & air purification systems

It is crucial to maintain the tank water at a high level of purity, since pollutants could absorb or scatter Cherenkov photons before they are detected. This transparency has to be consistent in time, as otherwise the energy reconstruction calibration would be too difficult. The removal of radioactive contaminants like radon is of special importance since they could travel far from the ID border into the fiducial volume, decay and contribute to the background, especially for low energy neutrinos.

For this purpose, SK water is continuously circulated through a **purification system** comprised of several resins and filters with a flow of around 60 tons/hour. The in and out points for this system have been chosen to minimize convection currents, which contribute to radioactive contaminants traveling inside the detector volume. Heat exchangers are used throughout the water purification system to maintain a temperature of 13 ± 0.01 C, which is monitored with eight thermometers with 0.0001 C precision. The low variability is helpful for further convection reduction. The low temperature suppresses bacterial growth and reduces PMT noise. UV sterilizers are also used to kill bacteria during the purification procedure. Radon-free air is dissolved in the SK water and then it is degasified, yielding a lower radon concentration afterwards.

The origin of the **radon gas** is the surrounding rock, from natural uranium decay. Aside from being a background source, it is a health risk for the workers. The air flow patterns on the underground laboratory change with each season, resulting in a large seasonal variation in the radon contamination, going from 30 Bq/m^3 in the winter to 1500 Bq/m^3 in the summer. To reduce the peak air contamination, a purification system was built, which pumps filtered air from outside into the mine. With the system in place, radon levels at experimental areas are < 40 Bq/m^3 all year round [52].

4.1.3 Electronics and data acquisition

In experiments with large data inputs like SuperK or LHC, trigger systems must be set for two reasons: reducing the total space needed to store all data and not overwhelm the data acquisition (DAQ) systems.

The system which was in place from SK-I to SK-III on the inner detector was called ATM (Analog Timing Module), which was an analog-to-digital converter, recording integrated charge and arrival times of each PMT signal. The first trigger was a hardware one and checked how many ID PMTs were hit and with how much total energy in a certain time window. Three thresholds existed: SLE (super low energy), LE (low energy) and HE (high energy). An OD trigger also existed for noticing heavy background activity.

In August 2008, the electronics and DAQ of SuperK were upgraded, with larger charge dynamic ranges and larger event rate capabilities. Every hit was recorded and filtered with software triggers, which can be more complex and precise than hardware ones. To have an order of magnitude intuition: the event rate for solar neutrinos in the SK ID is ~ 2 mHz, for background muons it is ~ 2.2 Hz, the SLE trigger rate in SK I-III was ~ 3 kHz and the event rate at ATLAS is around ~ 1 GHz. While even today the speed of hardware triggers is indispensable in LHC detectors, it was a logical improvement to remove them in Super Kamiokande.

Another objective of the electronics update was to store different event time widths for different trigger types. HE triggers happen at a much lower rate than SLE, so it is interesting to save data from before the trigger itself to capture any possible pre-activity. With all of this, the ATM system was replaced with the QBEE system (charge-to-time based electronics with ethernet). Under ATM, all triggers recorded 1.3 μs of data. Under QBEEs, SLE save 1.3 μs while both LE and HE save $-5 \rightarrow +35$ μs surrounding the trigger time.

4.1.4 Detector calibration

The detector calibration is crucial to the quality of the event reconstruction and all the subsequent physics analysis. Numerous parameters have to be obtained for the Monte Carlo simulations of the detector, so the detector responses can be accurately simulated and therefore it can be used to analyze the data with smaller systematic errors. Three main areas that need to be calibrated are PMTs, water transparency and energy reconstruction [34].

For PMTs, the charge and timing output needs to be understood and how it relates to the energy and time of the collected photons. In addition to that, each PMT must emit the same current for the same amount of incident light. As the detector isn't spherically symmetric, a light source in the middle doesn't yield the same light input in each PMT, so 420 PMTs were individually calibrated and

mounted in the tank to serve as reference for the uncalibrated ones.

A few aspects of the water tank need to be studied. First, to measure the light absorption and scattering in the water a laser is fired through an optical fibre and into the tank at various wavelengths, measuring various parameters in the ad-hoc models used in the Monte Carlo. The reflection of light on the PMT surfaces and the properties of the black sheet that divides ID from OD have to be studied as well, for which a similar laser setup is used.

Finally, energy scale calibration refers to knowing the original energy of the neutrino which produced a certain number of photoelectrons. A data vs Monte Carlo comparison is performed for event samples in energies from 50 MeV to 10 GeV, modifying the simulations for the best fit.

4.2 Physics of Gd doping

The SuperK-Gd project is the ongoing upgrade of the Super Kamiokande detector, which consists in dissoving Gd salt into the main water tank at a 0.2% concentration, as well as adapting the water filtration system and the simulations required for interpreting experimental data. Even though SK could already distinguish between neutrinos and antineutrinos at low energies due to their differences in scattering angle [12], the separation is greatly improved with neutron tagging.

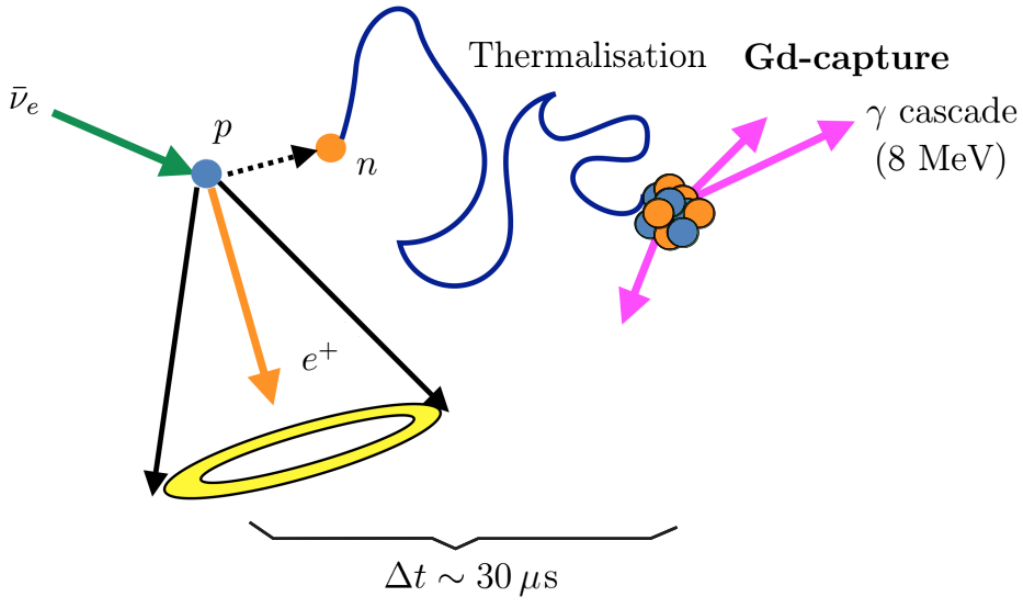

Figure 4.3: Diagram of an inverse beta interaction with Gd neutron tagging [51].

4.2.1 Neutron tagging mechanism

In regular water-Cherenkov detectors, free neutrons thermalise and get captured by protons in about $\sim$ 200 μs. This capture produces a single 2.2 MeV gamma ray which is very difficult to detect as there are many backgrounds at such low energies. However, some neutron tagging has been achieved in SK prior to Gd doping.

Gadolinium is a rare earth notable for its high neutron capture cross section. This cross section varies depending on the isotope and can go as high as 254000 barn for ^{157}Gd. When averaging all isotopes with their respective natural abundances, the resulting cross section is 48750 barn. This is very high, compared to 0.3 barn of hydrogen and $1.9 \cdot 10^{-4}$ barn of oxygen [69]. After the neutron capture, the nucleus is in an excited state so it emits a γ ray cascade and drops to the ground state. The number of photons and total energy varies depending on the isotope, but on average it's three to five photons with a total 8.05 MeV de-excitation energy. This characteristic signal topology is advantageous for the event reconstruction procedure.

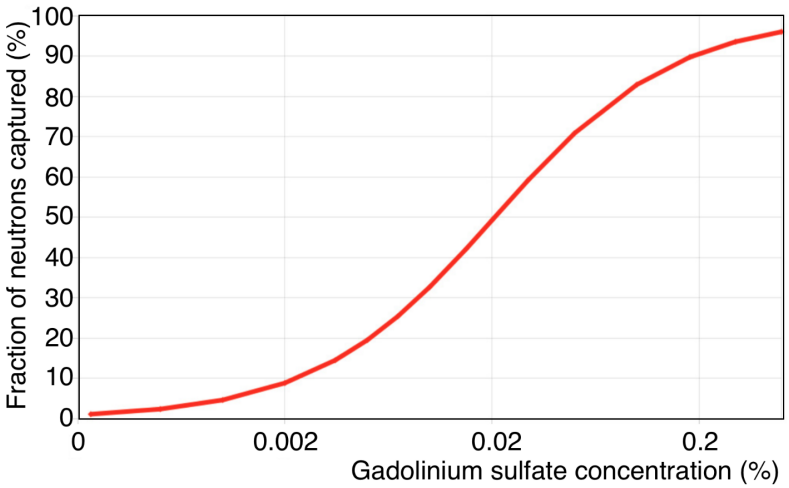

Figure 4.4: Fraction of neutrons captured by Gd as a function of its concentration [51].

The process is sketched in (Figure 4.3). First, a neutron is produced, in this case it was from an inverse β decay. The neutron thermalises with the surounding medium through elastic interactions in $\sim$ 10 μs, to then be captured by one of the Gd nuclei. The capture and de-excitation times are $\sim$ 20 μs, yielding a total of $\sim$ 30 μs delay between the Cherenkov light cone emission from the outgoing positron and the γ cascade. The distance between both events is $\sim$ 2 m, mainly due to the thermalisation process. At 0.2% concentration of Gd by mass, the fraction of captured neutrons is 90% while the total neutron tagging efficiency is slightly lower, at around 80% (Figure 4.4).

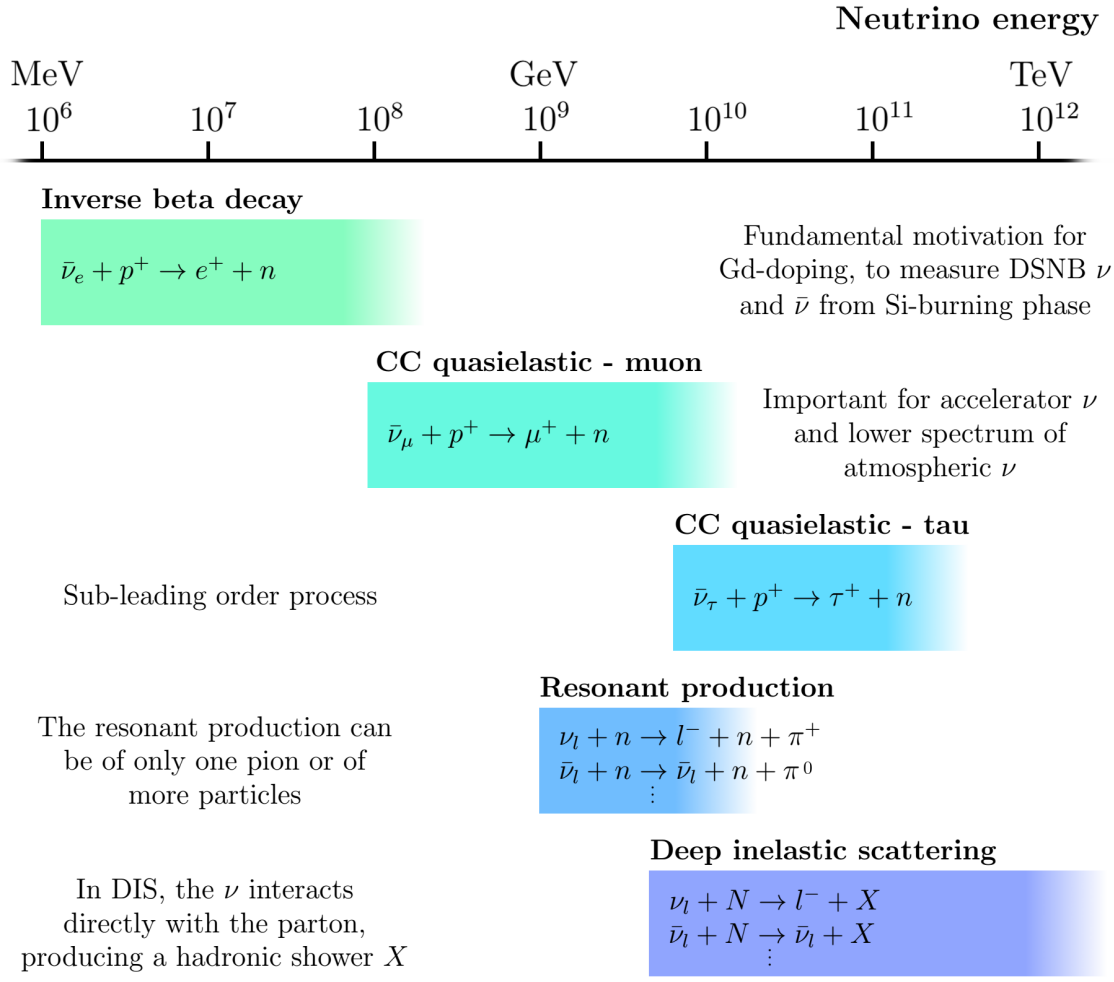

Important at high energies: secondary interactions

Secondary interactions inside the nucleus give rise to high n multiplicities.

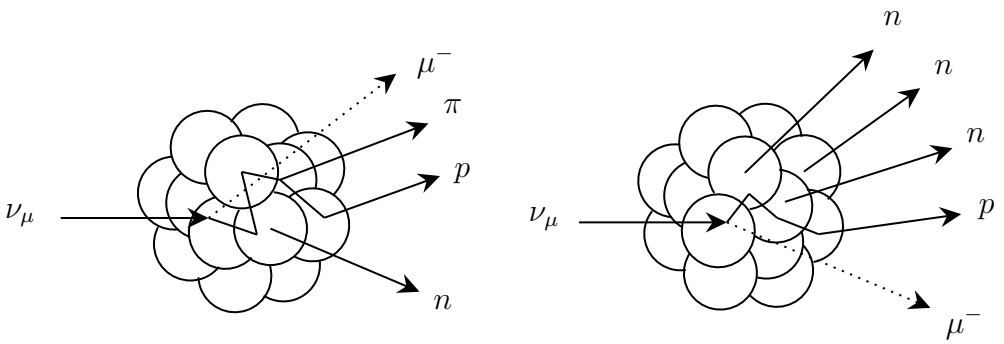

Figure 4.5: Sketch of the various neutrino-induced neutron producing processes as a function of neutrino energy. While for $10^6 - 10^8$ eV only inverse β decay can produce neutrons, for energies higher than 10^8 eV many other processes start taking place. In addition to those, secondary interactions inside the nucleus (mainly oxygen nucleus of the water) can give rise to high neutron multiplicities. Theoretical predictions and experimental measurements of neutrino cross section values as a function of its energy can be found in [28].

4.2.2 Neutron production mechanisms

Adding Gd will allow us to detect free neutrons in the water tank, but to extract the physics from that data we need to know about all neutron-producing processes in the experiment. This is strongly dependent on neutrino flavour, particle/antiparticle nature and energy.

From 1 to 100 MeV, only electron antineutrinos can produce neutrons. At **low energies** this feature provides a simple and efficient way of discerning antineutrinos from neutrinos and is the main motivation for the development of the project. This process should allow SK to be able to realize the first measurement of the DSNB and of the antineutrinos from the Si burning phase of a star. At higher energies the dynamics are much more complex, with more flavours and non-antineutrinos also producing neutrons. Information regarding the different high energy processes has been condensed in (Figure 4.5).

On the **high energy** regime, a challenge arises. Neutrino energy is reconstructed via the so called *visible energy*, defined as the sum of the energy of all the Cherenkov rings with the same vertex. However, visible energy doesn't take into account the energy transferred to the nucleus and transformed into neutral hadrons (η, κ, π, ...). This loss gets more relevant the higher the initial neutrino energy becomes. This also depends on the exchanged boson, as NC events leave larger energy fractions in the target. Neutron multiplicity helps in this task, as there is a correlation between energy transferred to the nucleus and neutron multiplicity.

4.3 Physics searches in SK & Gd doping potential

4.3.1 Solar & reactor

Neutrinos from both of this sources can be used for the determination of θ_{12}, θ_{13} and Δm^2_{21}. Around 200 events/day of solar neutrinos occur in SK. As we saw in (Table 3.2), low energy solar neutrino measurements are one of the most compromised in SuperK-Gd due to the new radioactive contamination of the Gd salt.

In SK, reactor antineutrinos are hidden under spallation product backgrounds [43] and solar neutrinos. With neutron tagging, they will be able to be distinguished due to their inverse β interactions. The expected rate of reactor antineutrinos in SuperK-Gd is 7.7 events/day [46]. Some radioactive backgrounds exist, but they are dim in comparison. With both solar and reactor datasets, the sensitivity to the solar oscillation parameters will be significantly enhanced.

4.3.2 Atmospheric & LBL

Even though the neutron production processes are more complex, Gd doping still improves the separation between ν and $\bar{\nu}$ from 100 MeV to 10 GeV. Since neutron multiplicities vary between NC, CC-DIS and other CC interactions, neutron tagging allows for better classification of atmospheric events. The neutron multiplicity is correlated to the fraction of the neutrino invisible energy, so it can be used as a correction in the energy reconstruction process. With these distinctions, the sensitivities to both δ_{CP} and the mass hierarchy are significantly improved.

4.3.3 Supernova Early Warning

For supernovas less than 1 kpc away, SuperK-Gd should be able to measure the neutrinos of its Si-burning stage. Assuming a very close one such as Betelgeuse (0.2 kpc away), $\sim$ 16.4 events/day are expected with an increasing flux as time approaches the core collapse. The background for this measurement is of $\sim$ 30 events/day, consisting mainly of reactor $\bar{\nu}$, being Gd radioactive backgrounds almost negligible. This measurement can be used as an early warning for optical observatories and also reports information about the dynamics prior to the core-collapse.

4.3.4 Supernova burst

In the case of a nearby supernova, the neutrino flux would be of the order of thousands of events. With neutron tagging, ν and $\bar{\nu}$ fluxes can be extracted independently. This flux is so high that the neutrino spectrum and time profile can be analyzed with negligible background.

4.3.5 DSNB

Althought neutrinos and antineutrinos of all flavours are produced in more or less the same amount, $\bar{\nu}_e$ are the most easy to identify after Gd doping. Prior to this update, the DSNB measurement in SK was background-limited, which implied that the precision increased as $\propto \sqrt{t}$, where t is the measurement time. Neutron tagging allows the almost complete reduction of spallation and free μ backgrounds. In energies above 10 MeV, where reactor antineutrinos are almost non-existent, the SuperK-Gd DSNB measurement precision will grow as $\propto t$.

The DSNB neutrinos come mainly from the core collapse (not Si-burning plase) and thus are emitted thermally. The mean of the thermal spectrum determines the shape of the spectrum. In (Figure 4.6), bands are shown for various temperatures, as well as a prediction supposing that all supernovas were like SN 1987A, which is unreasonable, as it is on the very low end of the thermal spectrum.

For SuperK-Gd, around 5 events/year are expected. The background above 10 MeV comes mainly from to the ^{238}U impurities in the salt, at around 0.11 events/year/(mBq/kg of ^{238}U). As we will see in the next chapter, the experiment requirement is < 5 mBq/kg of ^{238}U. Bounds have been set at 2σ such that the average contamination of all the dissolved Gd salt is < 10 mBq/kg, which results in around 1 event/year of background.

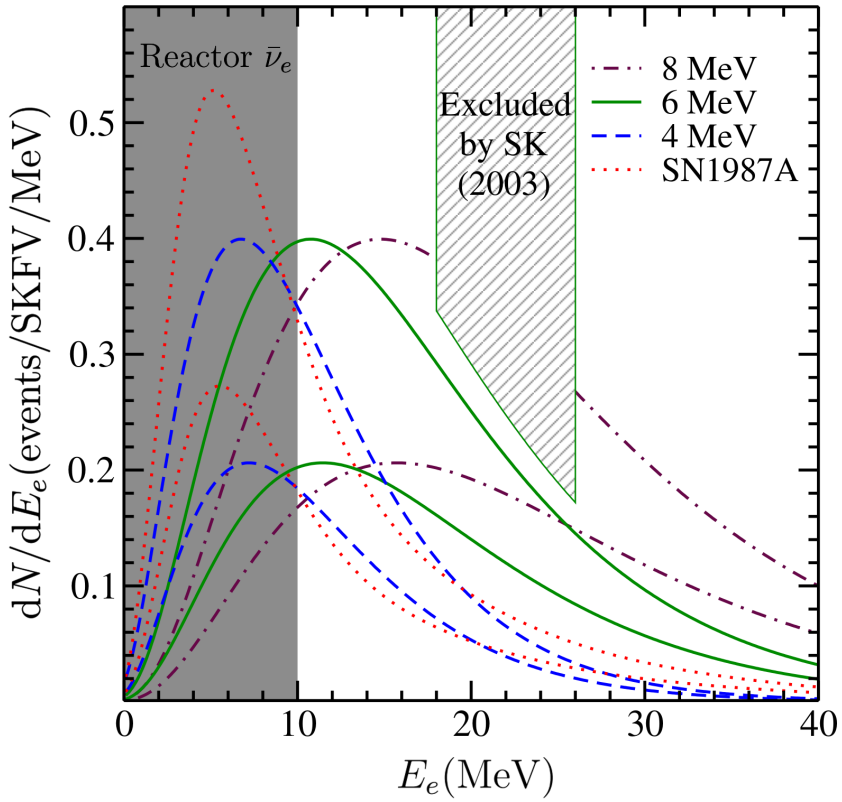

Figure 4.6: Predicted DSNB $\bar{\nu}_e$ event rate spectrum in the SK fiducial volume (FV) in the positron energy. The spread between different labeled temperature bands indicates the uncertainty in the supernova neutrino emission; the widths of the bands indicates the uncertainty in the cosmic supernova rate. The 2003 exclusion zone is shown, and the reactor $\bar{\nu}_e$-dominated zone shaded [25].

4.3.6 Proton decay

Baryon number symmetry has been observed to be an extremely good symmetry in nature and it is conserved in the SM at any order in perturbation theory. However, higher order (non-renormalizable) operators can be written which violate B and L but conserve $B-L$. Great unified theories (GUTs), which are well motivated, predict proton decay in a necessary manner, albeit with long lifetimes. Since SuperK is an enormous proton pool, one can test the various decay channels in the experiment.

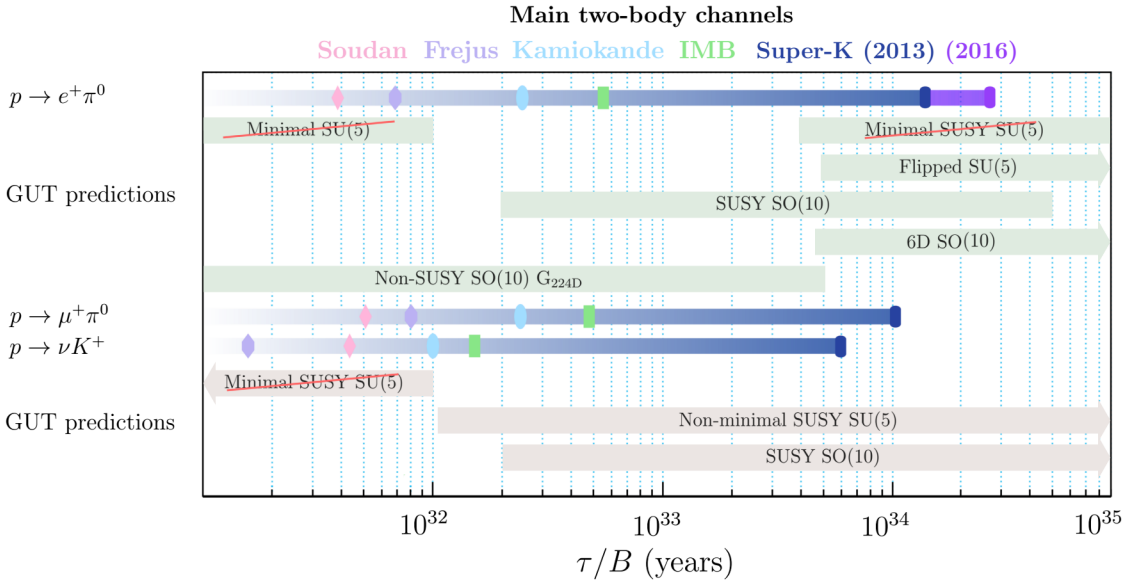

Figure 4.7: Summary of lifetime limits for the main $(B-L)$-conserving proton decay channels. Soudan, Frejus, Kamiokande, IMB and Super-K 2013 measurements are from [30], updated with GUT predictions from [59] and more recent Super-K measurements from 2016 [50].

So far, only bounds have been set (Figure 4.7), which have already excluded minimal SU(5) and minimal SUSY SU(5). Other tests which can be done are searching for $n \leftrightarrow \bar{n}$ oscillations [38].

Currently, SK can't distinguish events which have neutrons in their final states from those who don't. In SuperK-Gd a **neutron veto** allows for significant background reduction in searches where no final state neutrons are expected. In proton decay searches, this requirement removes 83% of the atmospheric neutrino background with negligible efficiency losses as protons are rarely expected to decay into neutrons.

4.4 Previous R&D - EGADS

One big milestone after the initial proposal of dissolving Gd in water-cherenkov detectors [21] was the construction and testing done in EGADS (Evaluating Gadolinium's Action on Detector Systems). The EGADS detector is designed similarly to SK but 250 times smaller and only with an inner detector. The project started with five goals:

- Show that Gd sulfate has no adverse effects on the SK components.
- Demonstrate that the purification system can achieve and maintain good water quality while keeping the Gd concentration constant.
- Demonstrate that adding Gd sulfate will not damage existing SK analyses.
- Study how to reduce the neutron background from spallation, U/Th fission chains in Gd sulfate impurities, ambient neutrons, etc.
- Prove that Gd can be added/removed in an efficient and economical way.

All of those goals were successfully achieved [69].

4.4.1 Gd salt corrosion

Gadolinium itself is insoluble in water but various ionic compounds can be used. Gd nitrate $Gd(NO_3)_3$ was quickly discarded since it is opaque in the UVA region, which covers a portion of the studied spectrum. Gd chloride $GdCl_3$ is easily soluble and has good Cherenkov light transparency, but component soak tests proved that it was slightly corrosive, which affects both component lifetime and water transparency. Finally, Gd sulfate $Gd_2(SO_4)_3$ was chosen, as it has similar solubility and transparency without the corrosion issues. This selection was done prior to EGADS construction, however EGADS proved that there wasn't anything unexpected with this compound. It is easier to dissolve when octahydrated, $Gd_2(SO_4)_3 \cdot 8H_2O$, however once dissolved most of it separates into ions, Gd^{3+} and SO_4^{2-}.

4.4.2 Water purification system

The SK water purification system produces ultrapure water with a resistivity close to the theoretical maximum, achieved after several stages of filters, UV lamps, reverse osmosis, vacuum and membrane degasifiers as well as resins, which remove impurities, ions and bacteria. This current system would instantly remove all the Gd salt if it were to be added. Thus, a new system which removed every impurity except Gd^{3+} and its anionic partner was mandatory. EGADS achieved this with a three stage water purification systems.

First, the Gd sulfate mixing and **pre-treatment** system, whose main function is to remove uranium and prepare the salt to be introduced into the main tank. Secondly, the **band-pass** system, which is EGADS' main filtration mechanism. With a series of nanofilters, it divides water into water with less than 1 ppm of Gd and the rest. The Gd-less water is then filtrated as usual, which then joins the concentrated Gd solution. Finally, the **fast recirculation** system consists on all filters which can't remove Gd and even though less powerful than the band-pass filtration, it allows the system to reach the required 90 liters/minute.

One key point about EGADS was also monitoring the Gd sulfate concentrations at all times, to see how much the water system removed. Various ports were used to regularly sample water from top, middle and bottom parts of the detector. In each sample, the Gd concentration was determined manually by using an Atomic Absorption Spectrometer.

4.4.3 Water transparency

Good water transparency ensures that low energy particles can be detected, and consistent water transparency makes the Monte Carlo simulations more reliable. A dedicated device was developed to measure it at EGADS, the UDEAL (*Underground Device Evaluating Attenuation Length*). It is composed by a vertical pipe of 8.6 m with an array of seven lasers, covering the main Cherenkov radiation spectrum from 337 nm (dark blue) to 595 nm (light green). These measurements are done at various water levels.

The EGADS program has proven how little effect Gd has on the water quality. While SK-III and SK-IV water transparency was $75\% - 82.5\%$, EGADS water transparency was around 5% less on average, while still being most of the time on the SK-IV ranges.

Adding Gd requires new parameters to be added on the Monte Carlo simulations, and thus new calibrations have to be done. The salt can both absorb or scatter the light. At 0.2% concentration, most of the loss was due to absorption and only 10% was due to scattering.

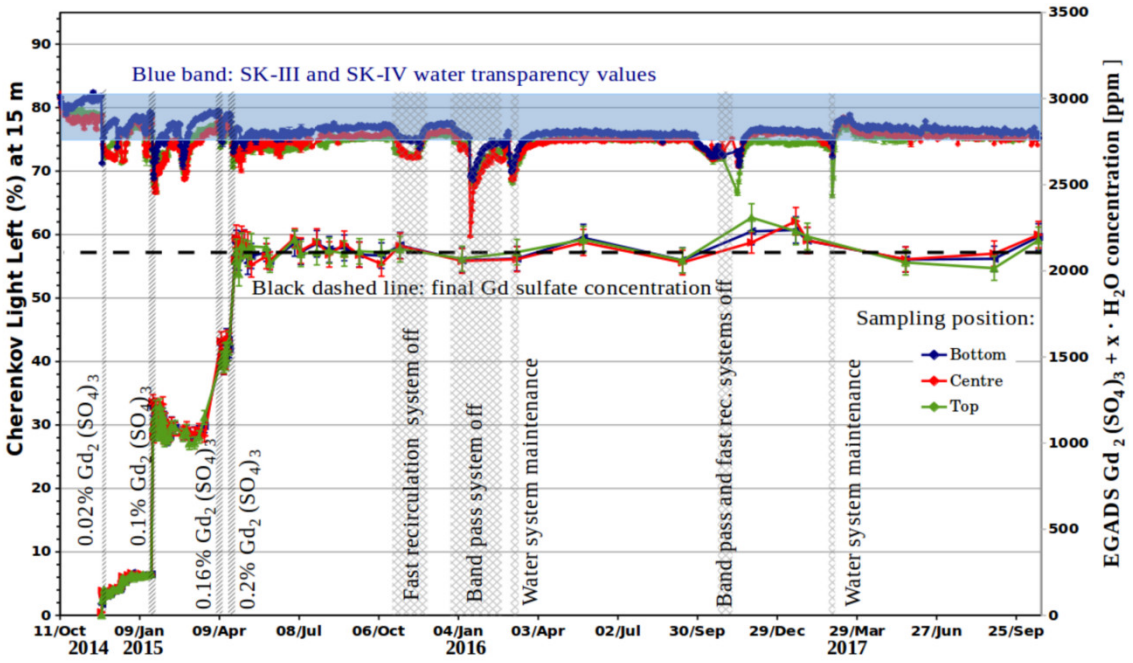

Figure 4.8: Upper three lines: Cherenkov light left [%] at 15 m (left y-axis scale), and lower three lines: Gd sulfate concentration for the three sampling positions in the EGADS detector (right y-axis scale). The line colors for the bottom, center and top sampling positions are blue, red and green, respectively. The blue band represents the typical Super-K ultrapure water transparency values while the horizontal dashed line represents the Gd sulfate final target concentration. Figure shown as seen in [69].

Chapter 5

The radiopurity program

The untapped physics potential of Gd-doping in Super Kamiokande is promising, but as we have already seen, the signals are dim so extreme care has to be put into reducing the new backgrounds. Thus, the radiopurity program was started. Comprised by new Monte Carlo studies, R&D with the producing companies and measurements of the impurities present in the Gd salt, all of those parts work together towards minimizing the possible negative effects on the experiment.

5.1 Detection efficiency problems from Gd doping

5.1.1 Radioactive background

Radioactive impurities in the salt are dissolved among the whole water tank, which is a background that can't be reduced just by limiting valid events to those on the fiducial volume.

After a radioactive nucleus decays, there are three different possibilities for its daughter: it may be unstable and decay, it may be stable and it may be in a long-time excited state. This last type emit photons of well defined energy when falling back to its ground state, which may as well be either unstable or stable. The emitted photons aren't always the same, as it is possible for the nucleus to decay before emitting them or falling multiple nuclear energy levels at once. However, the gamma emissions from decays are in most cases very well studied. Programs like JANIS are a comprehensive search tool for this information [33].

Successive unstable or metastable decays are called a **decay chain**. The most commonly observed ones are the four transuranic decays, where the first isotope is a heavy element with a very long half-life, similar or longer than Earth's age. Those are ^{232}Th, ^{237}Np, ^{238}U and ^{235}U. Of those, the neptunium chain is the least common in nature and it hasn't been observed in our experiments. A scheme of the other three as well as their emitted γ energies and half lives can be seen in (Figure 5.1).

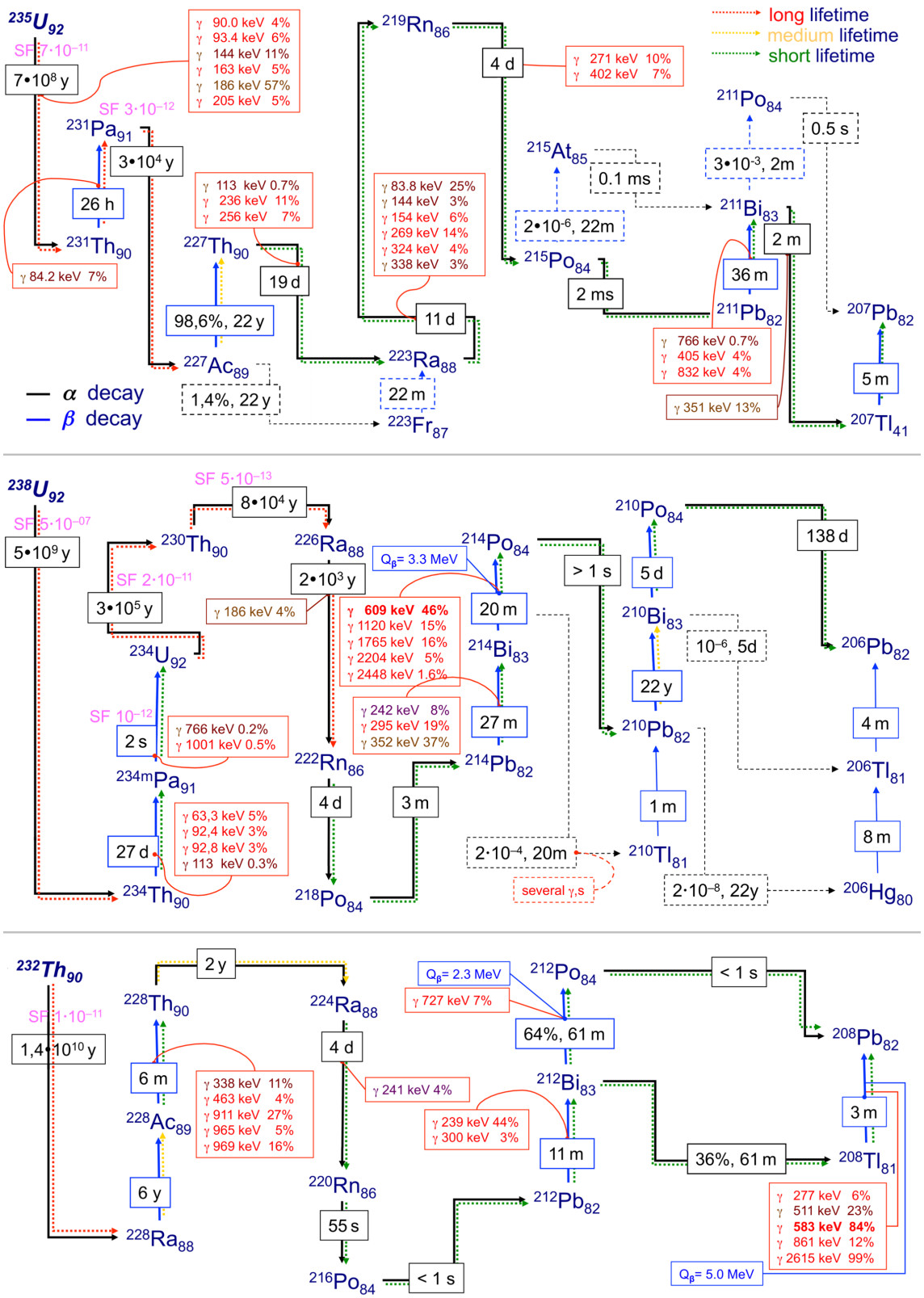

Figure 5.1: Main radioactive decay chains found as contaminants in the radiopurity program: Uranium 235, Uranium 238 and Thorium 232, with their half lives and most relevant gamma lines. Shown: energy, relative intensity and decay from which they come from.

Radiopurity requirements

For the SuperK-Gd experiment, bounds were calculated such that concentrations of those radioactive elements wouldn't suppose noticeable backgrounds [51]. Those are shown in (Table 5.1). Other contaminants aside from those on the main transuranic chains are studied. Isotopes like ^{60}Co are cosmogenic, produced when the stable material is exposed to cosmic rays. Others like ^{134}Cs and ^{137}Cs are produced after nuclear fission processes. In our case, the Fukushima accident is the biggest source of them, some past samples treated there having been contaminated. Others like ^{176}Lu and ^{138}La are commonly generated near rare earths, thus they are frequent contaminants in Gd samples.

Table 5.1: Radiopurity requirements for the three main chains, given in mBq/kg. When no number is given, its corresponding requirement is less restrictive [51].

Chain	**DSNB**	**Solar**
Upper ^{238}U	<5	-
Lower ^{238}U	-	<0.5
Upper ^{232}Th	-	<0.05
Lower ^{232}Th	-	<0.05
Upper ^{235}U	-	<30
Lower ^{235}U	-	<30

The chains have been explained as entire entities, however these bounds are given for low and high chains. In the case of ^{238}U there is a bottleneck towards the middle, as very fast decays are then followed by long lived isotopes, and then fast decays again. In nature, chains are usually in equilibrium given enough time, but in our samples the contaminant removal process doesn't remove all elements in the same way, thus leaving them in non-equilibrium.

A quick reminder about units and orders of magnitude. The Becquerel (Bq) is a unit for radioactive activity. Bounds are given in mBq/kg. One mBq/kg is 10^{-3} decays per second, per kilogram. Translated to concentrations, < 0.05 mBq/kg of ^{232}Th is equivalent to < 0.012 ppb (parts per billion).

High energy beta decays

The photons emitted in these decays can't be confused with Cherenkov photons, as those range the $337 - 595$ nm which correspond to $2 - 3$ eV, five to six orders of magnitude lower. However, photons in the ∼MeV range can be problematic, mostly as background to the lowest energy solar neutrinos measured by SK. As we can see in (Figure 5.1), some decays with problematic energies are ^{208}Tl, ^{214}Bi and ^{212}Bi.

Spontaneous fission

Spontaneous fission is a radioactive decay that can happen with heavy isotopes in the salt. In this process, the nucleus is split into various pieces, usually two of approximately equal weight plus a few neutrons. Concerning low energy neutrino physics, spontaneous fission of ^{238}U is the most relevant (as the one from ^{232}Th is four orders of magnitude less probable). In the spontaneous fission of uranium, various MeV photons are emitted as well as 2 neutrons of $1-2$ MeV. This is an irreducible background for DSNB, reactor, and supernova measurements.

(α, n)

This is a secondary process that can take place after an alpha decay, which occur most often in decay chains. The alpha particle can be captured by one of the oxygen nuclei in the water, producing two neutrons [51].

$$^{18}\mathrm{O} + \alpha \rightarrow {}^{22}\mathrm{Ne} \rightarrow {}^{20}\mathrm{Ne} + 2n \tag{5.1}$$

Those neutrons can take some of the lowest energy signals. Also, if in coincidence with a neutrino event, it could fake a $\bar{\nu}$ inverse beta interaction.

5.1.2 Fluorescence

Aside from radioactive processes, contaminants could also be a problem due to fluorescence. It is a form of luminiscence, in particular light emission of usually lower energy than the absorbed radiation and with a significant time delay. Altering the energy of the photons inside the water tank is an issue when reconstructing the initial energy of the particles and the time delay may produce fake signals.

To study fluorescence in materials, a **spectrophotometer** is used. It's an optical instrument which consists of a light source, a way to focus light onto the sample, a way of collecting the light afterwards, a monochromator to separate it into different wavelengths and a detector to measure the intensity at each wavelength. To obtain good fluorescence data, the materials have to be diluted in just the right amount, since being too diluted makes the fluorescence signal too dim and too much concentration can allow for the emitted light to be reabsorbed by the fluorophore, attenuating the signal. Scattered light gives rise to artifacts in the fluorescence spectra, which are seen as straight lines on the (excitation λ, emission λ) plane.

In these experiments, the most common fluorophore is **cerium**, which emits light at 350 nm. Cerium is very problematic and its concentration in the Gd salt can decide if a batch is good for use or not, as it is difficult to remove. Concentrations of more than 30-40 ppb can be problematic. Other contaminants like **europium** have also been studied, but their signals are dimmer (fluorescence hasn't been seen at <1000 ppm) and the $\lambda = 600$ nm is further away from the Cherenkov range.

5.2 Radioactivity determination techniques

Two techniques have been used for the radiopurity measurements: HPGe (high purity germanium) and ICPMS (inductively coupled plasma mass spectrometry).

5.2.1 Gamma spectroscopy - HPGe

Gamma spectroscopy measures photons emitted by radiactive materials. Nowadays, **germanium detectors** are used as they have the biggest photoelectric cross section and also have excellent energy resolution, allowing close peaks to be distinguished. The energy range covered can be from a few keV to MeV, but energies that high aren't necessary for radiopurity measurements. At very low energies (<200 keV) there are several interesting peaks, but the background at those energies is very high and difficult to predict, limiting the effective energy range of the detectors [24].

There are many types of Ge detectors, and the way in which they are built determines how the data must be analyzed (as different Monte Carlo simulations have to be used) and also the appearance of certain artifacts, like spurious peaks due to photon reflection. Those kinds of artifacts don't appear in the HPGe detectors at Canfranc, the ones that we used for this thesis and which we will explain now.

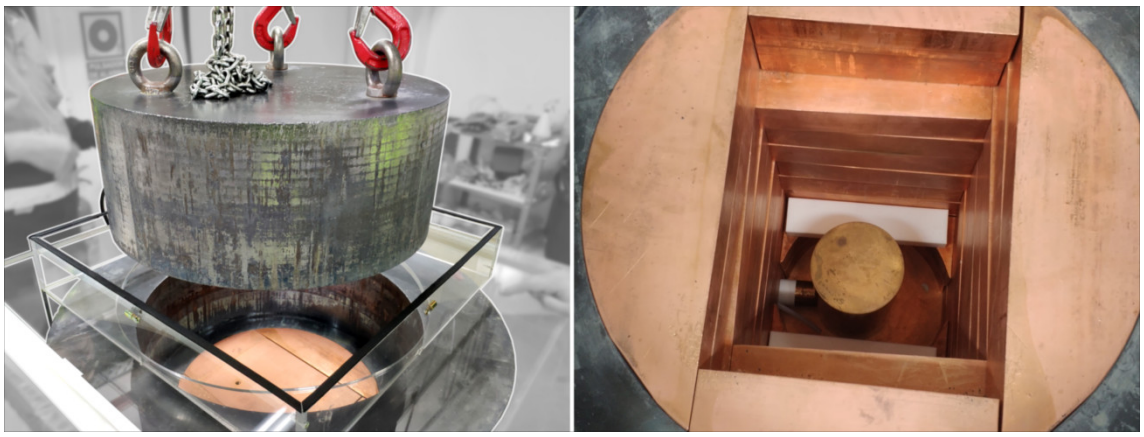

Figure 5.2: One of the HPGe detectors at Canfranc. On the left, the several ton Pb lid being lifted by a crane installed in the room. The various layers of the detector (methacrylate outer cover for Rn-free air, outer & inner Pb layers and the innermost Cu layer) can be seen. On the right, we see the exposed copper bricks, two teflon slabs for lifting the samples as well as the HPGe cylinder itself. Photos took on late 2019 with permission of the Canfranc Underground Laboratory.

The central piece is an ultrapure Ge cylinder. It has to be cooled to 77K with liquid nitrogen which is kept in a dewar in thermal contact with the detector. This is then shielded by various layers of copper and lead in varying degrees of purity (Figure 5.2) to prevent cosmic muons from entering the detection volume. Adding more shielding after a certain point starts being inefficient since cosmogenic radioisotopes on the shielding contribute to the background more than diminish it.

Just like the Kamioka mine, Canfranc is underground and thus radon concentrations in the air are high. To avoid them from entering the detector, a methacrylate cover is installed over each detector and **radon-free air** is pumped inside it at a pressure higher than the one on the room [48]. Even though all data since day one of measurement is recorded, the first four to six days are usually discarded, until airborne radon concentrations are low enough. The measurements presented in this thesis are only from those radon-free days.

Measurement procedure

The procedure has to be very clean for not contaminating the sample, and also consistent between samples in order to have reliable MC simulations for the detector efficiency as a function of energy. For this, Marinelli containers are used, which are made so to suround the HPGe cylinder (Figure 5.3).

Figure 5.3: On the left, a Marinelli container holding $\sim$ 5 *kg of Gd salt about to be measured. Its interior hole is sketched over the photo in white dashed lines. On the right, the container set in the detector, surounding the HPGe cylinder. Photos took on late 2019 with the permission of the Canfranc Underground Laboratory.*

Signal and bound calculation

For interpreting HPGe spectra we need to know about the **interactions with matter** (the Ge cylinder and the Gd salt itself) of the gamma rays. They are mostly via photoelectric effect at low energies and Compton scattering at medium and high energies. The anatomy of energy peaks can be very complex, as the interactions depend on the energy on the photon and in addition to that, more detailed structures appear with higher photon counts [52]. However, the samples are so radiopure that in most cases structures like compton continuums, single & double escape peaks and so on can't be seen. In this case we are just looking for an excess of the photon count at a certain energy, which corresponds to the energy the photon was initially emitted at. If no signal is seen, bounds can be set.

A sample is usually measured for 30 to 50 days uninterrupted (t_{signal}). To be able to determine the excess of counts, another data run is taken without the sample, for a similar number of days t_{bkg}. The background is then normalized to match the measurement time of the sample. This background is different for each detector, but is more or less constant in time.

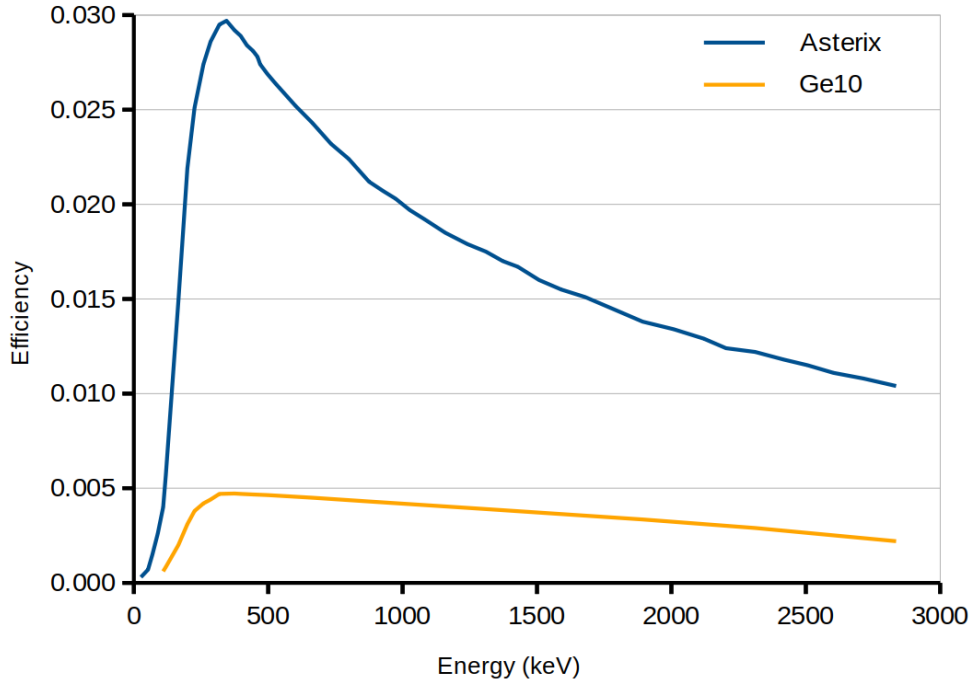

Figure 5.4: Simulated detector efficiencies for 5 kg Gd sulphate samples in Canfranc's Asterix detector, blue line [52] and HADES' Ge10, orange line [internal communication]. The uncertainty for the Monte Carlo simulation is about 10%.

To interpret the data, a Monte Carlo simulation for the efficiency has to be done. This takes into account the topology of the detector and the way the sample is located inside of it. Simulated detector efficiencies for one of the detectors in Canfranc Underground laboratory and one of HADES' detector −which was also used in the screening process− are shown in (Figure 5.4). The data also has to be calibrated, assigning the correct energies to each of the data bins. While calibration runs are done with elements like ^{60}Co and ^{152}Eu, I usually take the data from the first few days and calibrate using the ^{214}Bi peaks, which are many and abundant as bismuth is one of the daughter nuclei of the airborne radon.

At this point, we can already plot the full spectra of a sample. For example, in (Figure 5.5) the emission from one of the Gd samples can be seen.

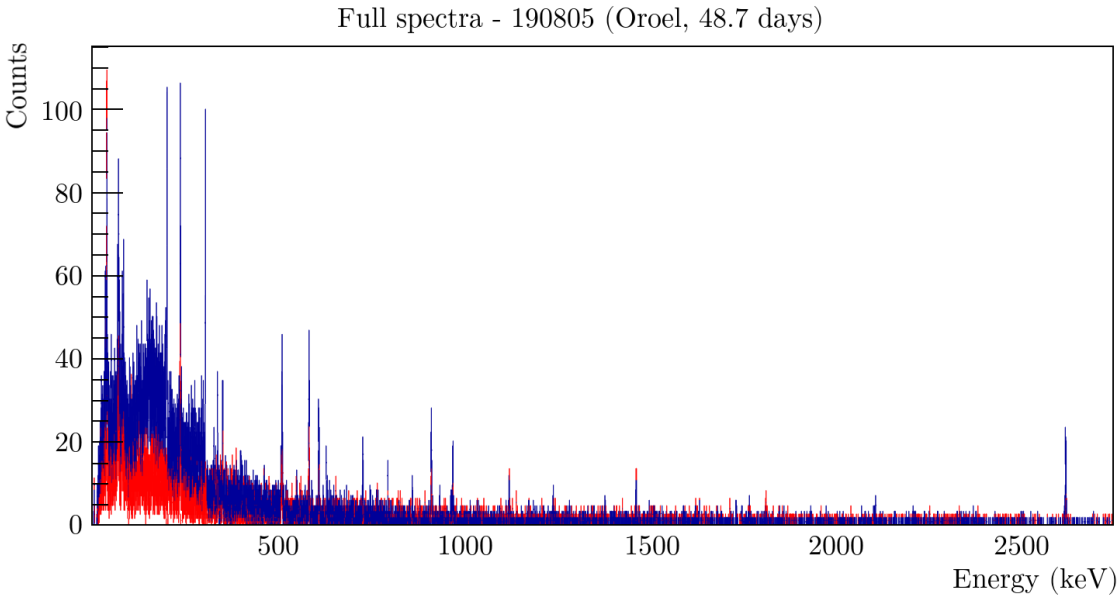

Figure 5.5: Radioactive spectra of the Gd sample 190805 after 48.7 days of measurements in Ge-Oroel, Canfranc. In blue, the signal, in red, the normalized detector background.

Once calibrated, we look at each energy where a relevant gamma peak might be found. The spectra is manually inspected each time in case any peak outside of the usual ones is seen. A code in ROOT which analyzes 99 gamma lines was developed, with an example output shown in (Figure 5.6). Signal (S) and background (B) data are shown with their respective errors as blue and red lines. Nearby energies where peaks might be found are tagged with vertical dashed lines. Two zones are highlighted, a blue zone, used for peak measurements (S_{peak}, B_{peak}) and a red zone, used for compton measurements (S_{compton}, B_{compton}), hand chosen for each energy in a way to avoid overlapping with nearby peak energies. The photon counts are then summed in both areas Our objective is to obtain a value for the radioactive signal (in mBq/kg) and if that's not possible, to set a bound, in both cases at 95% certainty (2σ). For that, the following equations are used, in which the background counts have already been normalized with $t_{\text{signal}}/t_{\text{bkg}}$ [14]

$$\text{[Net signal]} \qquad S_{\text{net}} = (S_{\text{peak}} - S_{\text{compton}}) - (B_{\text{peak}} - B_{\text{compton}}) \tag{5.2}$$

$$\text{[Detection limit]} \qquad L_d = 2.86 + 4.78\sqrt{S_{\text{compton}} + B_{\text{peak}} + 1.36} \tag{5.3}$$

- If $S_{\text{net}} < 0 \implies L_d$ is taken as upper limit.
- If $0 < S_{\text{net}} < L_d \implies L_d + S_{\text{net}}$ is taken as upper limit
- If $L_d < S_{\text{net}} \implies$ A signal was found with L_d being its uncertainty.

This yields either a signal or a bound in number of counts, to convert it to mBq/kg:

$$\text{Activity (mBq/kg)} = \text{Activity (counts)} \cdot \frac{10^3}{I \cdot \varepsilon \cdot t_{\text{signal}} \cdot m_{\text{sample}}} \tag{5.4}$$

where I is the line intensity (tabulated in JANIS), ε the detector efficiency at that energy from the Monte Carlo, t_{signal} the measurement time in seconds and m_{sample} the sample mass, usually 5 kg. Each subchain and isotope has many lines which can be analyzed, but the one which constrains the measurement the most is usually the same. The lines used are shown in (Table 5.2).

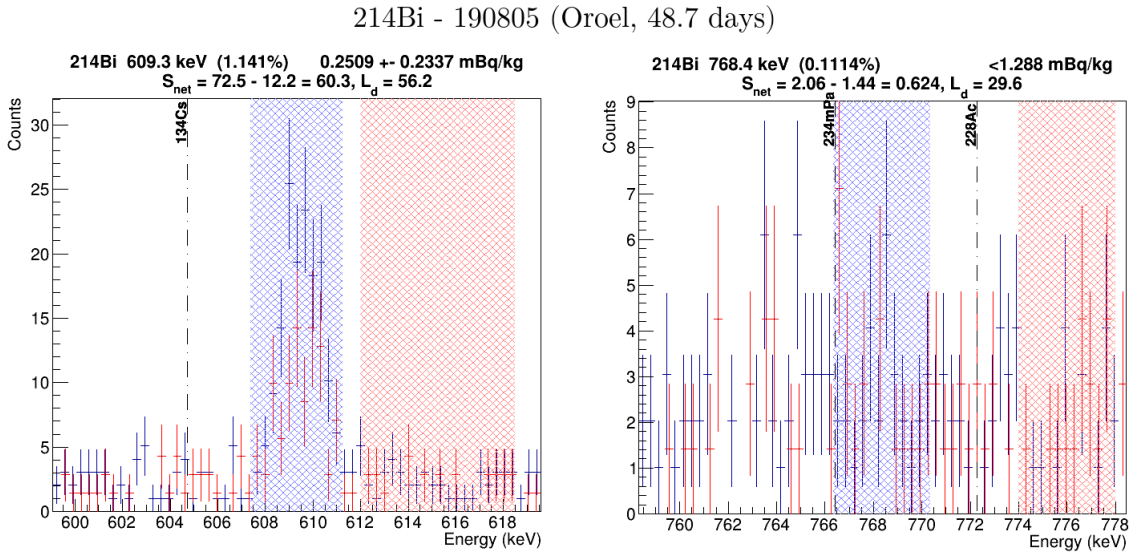

Figure 5.6: Two energies in which ^{214}Bi peaks can be found, 609 keV and 768 keV, together with experimental data of the Gd sample 190805 after 48.7 days of measurements in Ge-Oroel. The blue shadowed zone indicates the energy range in which peak energies are integrated and the red one, peak-free compton background. A signal, although dim, of 0.25 ± 0.23 mBq/kg was extracted from the left data, while only bounds can be set from the right one, as it is less intense.

5.2.2 Mass spectroscopy - ICPMS

In mass spectroscopy techniques, mass to charge ratio is measured, obtaining the concentrations (in ppm, for example) of each element. Most commonly available mass spectrometer can't distinguish between different isotopes, and only do distinguish one element from another. There are many ways of extracting the ions for the measurement, in our case we use inductively coupled plasma (ICP) sources. For this, the sample is dissolved, nebulized and then turned into ions by the plasma.

While ICPMS doesn't substitute HPGe measurements, it can serve as a double check and is also very useful for detecting concentrations of elements like Ce which aren't radioactive, but are fluorescent. For SuperK-Gd, we have analyzed some samples at various research centers, being the one at UAM-SIdI (Servicio Interdepartamental de Investigación) the one who yielded the best results.

Table 5.2: Compiled results for the samples assigned to Canfranc laboratory up to June 2020. Shown, 95% confidence level bounds and signals in mBq/kg for both upper and lower subchains of the ones described in (Table 5.1) as well as five other relevant radiactive contaminants. Aside from the measurements from Canfranc, data from HADES and Kamioka are shown too when available for this set of samples.

#	Lab.	Detector / technique	Ge, main chains (mBq/kg 95% c.l.)						Ge, other (mBq/kg 95% c.l.)				
			^{238}U△	^{238}U▽	^{232}Th△	^{232}Th▽	^{235}U△	^{235}U▽	^{40}K	^{138}La	^{176}Lu	^{134}Cs	^{137}Cs
		Chosen γ line (keV) →	1001.0	609.3	911.2	583.2	185.7	236.0	1460.8	1435.8	306.8	795.9	661.6
		γ line element →	^{234*}Pa	^{214}Bi	^{228}Ac	^{208}Tl	^{235}U	^{227}Th	^{40}K	^{138}La	^{176}Lu	^{134}Cs	^{137}Cs
		Experimental requirement →	< 5	< 0.5	< 0.05	< 0.05	< 30	< 30	-	-	-	-	-
190302	Canfranc	ge-Asterix	< 9.8	< 0.32	< 0.35	< 0.29	< 0.42	< 0.92	< 1.6	0.26 ± 0.1	< 0.21	< 0.09	< 0.09
	HADES	Ge10+Ge11	< 105	< 8.6	< 3.3	< 3.6	< 5.6	< 10.4	< 8.8	< 1.66	< 2.47	-	< 0.93
190303	Canfranc	ge-Asterix	< 8.4	< 0.3	< 0.44	< 0.29	< 0.39	< 0.81	< 1.5	0.45 ± 0.09	0.16 ± 0.12	< 0.08	< 0.09
190304	Canfranc	*(t.b.m.)*	-	-	-	-	-	-	-	-	-	-	-
	HADES	Ge10+Ge11	< 88	< 7.7	< 2.6	< 3.3	< 5.0	< 9.5	< 10	1.34 ± 0.96	< 1.28	-	< 1.26
190305	Canfranc	ge-Asterix	< 9.0	< 0.34	< 0.36	< 0.30	< 0.41	< 0.90	< 1.6	0.5 ± 0.1	0.14 ± 0.13	< 0.09	< 0.12
190601	Canfranc	ge-Asterix	< 10.2	< 0.52	< 0.35	< 0.41	< 0.50	< 1.36	< 1.90	< 0.16	1.25 ± 0.14	< 0.10	< 0.11
	Kamioka	*RaEmporeDisk*	-	< 0.32	< 0.39	< 0.34	-	-	-	-	-	-	-
190602	Canfranc	ge-Tobazo	< 29	< 0.49	< 1.64	< 0.82	< 0.76	< 1.85	< 2.10	< 0.21	1.64 ± 0.20	< 0.17	< 0.14
	Kamioka	*RaEmporeDisk*	-	< 0.28	< 1.01	< 0.28	-	-	-	-	-	-	-
190603	Canfranc	ge-Anayet	< 25.95	< 0.45	< 1.03	< 0.76	< 0.58	< 2.02	< 1.58	< 0.18	1.71 ± 0.14	< 0.15	< 0.12
190607	Canfranc	ge-Oroel	< 7.2	< 0.30	< 0.79	< 0.42	< 0.30	< 0.96	< 1.59	< 0.18	< 0.13	< 0.12	< 0.09
190608	Canfranc	ge-Asterix	< 8.8	< 0.53	< 0.43	< 0.35	< 0.40	< 0.88	< 1.50	< 0.14	< 0.25	< 0.08	< 0.09
	Kamioka	-	< 20.4	-	< 1.22	< 0.71	< 3.4	< 1.6	-	-	< 0.45	-	-
	Kamioka	*RaEmporeDisk*	-	< 0.49	< 0.43	< 0.55	-	-	-	-	-	-	-
190702	Canfranc	ge-Oroel	< 11	< 0.45	< 1.11	< 0.50	< 0.37	2.4 ± 0.9	< 1.50	< 0.20	0.23 ± 0.13	< 0.12	< 0.11
	Kamioka	-	< 9.4	< 0.57	< 0.97	< 0.26	< 2.6	< 1.4	-	-	< 0.44	-	-
190703	Canfranc	ge-Asterix	< 8.4	< 0.35	< 0.51	< 0.50	< 0.45	1.8 ± 1.0	< 1.70	< 0.20	0.51 ± 0.13	< 0.10	< 0.10
190801	Canfranc	ge-Anayet	< 28	0.39 ± 0.32	< 1.5	< 0.77	< 0.80	< 1.17	< 1.44	< 0.18	2.7 ± 0.2	< 0.23	< 0.18
190803	Canfranc	ge-Asterix	< 7.0	< 0.31	0.39 ± 0.21	0.55 ± 0.22	< 0.36	< 0.71	< 1.4	< 0.09	3.5 ± 0.1	< 0.08	< 0.07
190805	Canfranc	ge-Oroel	< 8.39	0.25 ± 0.23	0.53 ± 0.39	0.60 ± 0.36	< 0.40	< 0.89	< 1.12	< 0.09	9.38 ± 0.09	< 0.10	< 0.08
	Kamioka	IPMU-P	< 103	< 1.6	< 3.2	< 4.9	< 16	< 7.0	< 18	-	8.83 ± 0.82	-	< 1.2
190901	Canfranc	ge-Asterix	< 6.85	< 0.27	0.48 ± 0.23	0.34 ± 0.24	< 0.42	< 1.09	< 1.31	< 0.13	4.87 ± 0.11	< 0.09	< 0.12
	Kamioka	-	< 110	< 2.3	< 2.9	< 2.1	< 14.9	< 12.2	< 27	-	5.6 ± 0.7	-	< 1.1
190903	Canfranc	ge-Asterix	< 8.88	< 0.37	0.59 ± 0.28	0.35 ± 0.28	< 0.54	< 1.72	< 1.50	< 0.14	4.89 ± 0.13	< 0.10	< 0.09
	Kamioka	-	< 69	< 6.3	< 4.0	< 2.4	< 17.6	< 5.3	< 32	-	5.4 ± 0.8	-	< 1.0

5.3 Canfranc measurements for SuperK-Gd

For the SuperK-Gd project, several ktons of Gd salt have been comissioned. These are realized in 500 kg batches, of which 20 kg are separated. 5 kg are sent to a low background laboratory outside of Kamioka, either Canfranc or Boulby, while the rest are kept at Kamioka for HPGe measurements or stored for possible future studies. Canfranc and Boulby each share about 50% of the SuperK-Gd samples.

In (Table 5.2) the Canfranc HPGe measurements as well as their corresponding analyses from Kamioka are shown. These measurements haven't been published previously as they are part of the internal Collaboration material. For the rows marked with *Kamioka*, both the measurements and their analysis come from the Kamioka Observatory.

5.4 Analysis of the results

The interpretation of (Table 5.2) needs to be done in the context of the whole experiment, together with the data from Boulby, Kamioka and ICPMS. Only with all the data one can decide if the average radiopurity is good enough, which samples should be excluded and so on. This analysis has been realized in-depth by the Collaboration as a whole, which resulted in various decisions being taken, as we will now explain. The reader must be aware of the fact that this is the Collaboration's first approximation to the problem and thus things could change in the future.

First of all, we can see how **most of the samples are radiopure enough** and the measurements satisfy the experimental requirements. In some cases like the ^{238}U upper bound, the requirements couldn't be achieved since that would take several months of measurement time or even new detectors, neither being valid options at the moment.

In various samples (190803, 190805, 190901 and 190903) we have seen **high levels of ^{176}Lu**. The presence of this impurity −even in relatively high amounts like it is the case right now− doesn't suppose a big risk to the project. The energy of the emitted gammas is not problematic and ^{176}Lu doesn't have relevant fluorescent properties. However, we found a correlation between high ^{176}Lu concentration and ^{232}Th signals, which are problematic.

The upper ^{232}Th subchain is measured with a gamma line from ^{228}Ac, which decays with a half life of 6 minutes. This means that the measured ^{228}Ac activities will be the same for **^{228}Ra**, its parent nuclei. The concentration of ^{232}Th −the previous element in the chain− has been measured with ICPMS and it was seen to be low, under the experimental requirements. Thus, we conclude that the contamination is mainly due to ^{228}Ra.

5.5 Impact and course of action

Our recent findings about the relatively high **^{228}Ra** contamination in various samples are a challenge for the project. While they don't affect the DSNB measurements, they do damage the low energy solar neutrino precision and thus it's in our best interest to solve this issue for the final loading.

Currently, about 14 tons of Gd salt have been produced and analyzed. Around half of those batches show non negligible contamination of ^{228}Ra. The resins in the water purification system can remove $\sim$ 90% of the ^{228}Ra in the dissolved salt. Taking that into account, the **backgrounds can be estimated**: if only the most radiopure samples were to be loaded in this first phase it would induce a solar background of $6 - 12$ events/day in the fiducial volume and it would allow for 30% neutron capture efficiency. Loading all the gadolinium we currently have would up that background to $55-62$ events/day at 50% neutron capture efficiency. We should keep in mind that there are around 200 solar events/day. ^{228}Ra has a half life of 6 years so it wouldn't decay significantly in the timespan of the experiment. If it were to be completely removed, the next long-lived isotope in the chain, ^{228}Th, has a lifetime of 2 years so in that time period, the radioactive backgrounds would be reduced by a factor two.

In the end, the new backgrounds of $\sim$ 50 counts/day are acceptable, so it has been decided to load the whole 14 tons at this first stage. However, if the remaining 85 tons were to have the same amounts of radium, it would be too damaging for solar measurements. Thus, a **R&D project** has been set in motion to develop new techniques for salt re-purification and radium removal.

Chapter 6

Conclusions

About ninety years have passed since the first postulation of neutrinos and they still remain as **one of the least known sectors** in the standard model. What makes them so difficult to measure is also their main potential for physics, as they are direct probes into the inner workings of astrophysical phenomena, the interior of stars and the very first instants of the Universe.

For theoretical physicists, neutrino physics discoveries are crucial. Galactic and extragalactic fluxes, their masses and hierarchy, existence and number of sterile neutrinos, their Majorana or Dirac nature and the values of the parameters and δ_{CP} in particular are all key points for model building. Water Cherenkov detectors like Super Kamiokande have proven to be an invaluable tool in their study.

There are various challenges when loading Gd in water Cherenkov detectors like increased backgrounds, cost and the need for more advanced water purification systems. Nevertheless, the advantages of being able to tag neutrons, which in turn allows to distinguish between neutrinos and antineutrinos more precisely than before is a **breakthrough for neutrino physics** as it could enable the first ever measurement of the diffuse supernova neutrino background and better precision measurements of δ_{CP} and the mass hierarchy.

A preliminar experiment was built: EGADS, 250 times smaller than SuperK in which the Gd loading has been successful. We have calculated how important radiopurity measures are to these projects. For this matter, we are studying in detail each of the gadolinium salt batches. Samples of the first 14 tons of Gd salt have been thoroughly screened for their radioactive impurities, most of the time only being able to set bounds of their concentrations and in many cases being able to satisfy the experimental requirements for minimum background. Some of the samples have shown non negligible ^{228}Ra contamination, which isn't a problem at the moment but will be if those levels persist in the remaining 85 tons. Thus, a **new R&D program** was set in place to develop new ^{228}Ra removal techniques.

During the next decade the detector will be put to the test and its **great potential** will be realized. Current efforts will also help in the preparations of the possible Gd loading in future water Cherenkov detectors like HK, which could improve the measurements of SuperK-Gd by one or two orders of magnitude.

Epilogue

Neutrino physics is a rapidly evolving field and SuperK-Gd could change the future of neutrino experimental physics if successful. A new experiment in the Kamioka Observatory, Hyper Kamiokande, has already been approved and its construction has started. The HK fiducial volume is $\sim$10 times bigger than Super Kamiokande and if Gd loading is successful in SK we could see a HyperK-Gd in the future, with the implication of improving in one or two orders of magnitude all SuperK-Gd measurements.

Bibliography

[1] C.L. Cowan et al. - *Detection of the Free Neutrino: a Confirmation*, Science, **124**, 103 (1956)

[2] T. D. Lee, C. N. Yang - *Question of Parity Conservation in Weak Interactions*, Phys. Rev. **104**, 254 (1957)

[3] G. Danby et al. - *Observation of High-Energy Neutrino Reactions and the Existence of Two Kinds of Neutrinos*, Phys. Rev. Lett. **9**, 36 (1962)

[4] K. A. Olive, M. S. Turner - *Cosmological bounds on the masses of stable, right-handed neutrinos*, Phys. Rev. D **25**, 213 (1982)

[5] K. S. Hirata et al. (Kamiokande-II collaboration) - *Observation of a neutrino burst from the supernova SN1987A*, Phys. Rev. Lett. **58**, 1490 (1987)

[6] J. N. Bahcall - *Neutrino Astrophysics*, Cambridge University Press (1989)

[7] G. S. Abrams et al. (MARK-II collaboration) - *Initial measurements of Z-boson resonance parameters in e^+e^- annihilation*, Phys. Rev. Lett. **63**, 724 (1989)

[8] R. Frey (MARK-II collaboration) - *The Z^0 resonance in e^+e^- annihilation*, Theoretical Advanced Summer Institute Boulder, Colorado, (1989)

[9] K. S. Hirata et al. (Kamiokande-II collaboration) - *Observation of a small atmospheric ν_μ/ν_e ratio in Kamiokande*, Phys. Lett. B, **280**, 146 (1992)

[10] F. Halzen, B. Keszthelyi, E. Zas - *Neutrinos from primordial Black Holes*, Phys. Rev. D, **52**, 3239 (1995)

[11] T. Kajita - *Atmospheric neutrino results from Super-Kamiokande and Kamiokande - Evidence for ν_μ oscillations* - Nucl. Phys. Proc. Suppl. **77**, 123 (1999)

[12] P. Vogel, J. F. Beacom - *The angular distribution of the reaction $\bar{\nu}_e + p \to e^+ + n$*, Phys. Rev. D, **60**, 053003 (1999)

[13] S. Fukuda et al. (SK collaboration) - *Tau Neutrinos Favored over Sterile Neutrinos in Atmospheric Muon Neutrino Oscillations*, Phys. Rev. Lett. **85**, 3999 (2000)

[14] C. Hurtgen, S. Jerome, M. Woods - *Revisiting Currie: how low can you go?*, Appl. Radiat. Isot. **53**, 45 (2000)

[15] DONUT collaboration - *Observation of Tau Neutrino Interactions*, Phys. Lett. B, **504**, 218 (2001)

[16] SNO Collaboration - *Measurement of the rate of* $\nu_e + d \rightarrow p + p + e^-$ *interactions produced by* ^8B *solar neutrinos at the Sudbury Neutrino Observatory*, Phys. Rev. Lett. **87**, 071301 (2001)

[17] I. V. Anicin - *The neutrino. Its past, present and future* SFIN year XV, Series A: Conferences, **A2** 3-59 (2002)

[18] S. Fukuda et al. (SK collaboration) - *The Super-Kamiokande detector*, Nucl. Instrum. Meth. A, **501**, 418 (2003)

[19] P. Antonioli et al. (SNEWS group) - *SNEWS: the SuperNova Early Warning System*, New J. Phys. **6**, 114 (2004)

[20] Y. Ashle et al. (SK collaboration) - *Evidence for an oscillatory signature in atmospheric neutrino oscillation*, Phys. Rev. Lett. **93**, 101801 (2004)

[21] J. F. Beacom, M. R. Vagins - *GADZOOKS! Antineutrino Spectroscopy with Large Water Cerenkov Detectors*, Phys. Rev. Lett. **93** 171101 (2004)

[22] J. Lesgourges, S. Pastor - *Massive neutrinos and cosmology*, Phys. Rept. **429**, 307 (2006)

[23] M. C. González-García, M. Maltoni - *Phenomenology with Massive Neutrinos*, Phys. Rept. **460**, 1 (2008)

[24] G. Gilmore - *Practical gamma-ray spectrometry*, Wiley (2008)

[25] S. Horiuchi, J. F. Beacom, E. Dwek - *The Diffuse Supernova Neutrino Background is detectable in Super-Kamiokande*, Phys. Rev. D **79**, 083013 (2009)

[26] J. F. Beacom - *The Diffuse Supernova Neutrino Background*, Ann. Rev. Nucl. Part. Sci. **60**, 439 (2010)

[27] C. Spiering - *Towards high-energy neutrino astronomy. A historical review*, arXiv:1207.4952 [astro-ph.IM] (2012)

[28] J. A. Formaggio, G. P. Zeller - *From eV to EeV: Neutrino cross sections across energy scales* Rev. Mod. Phys. **84**, 1307 (2012)

[29] S. M. Adams et al. - *Observing the Next Galactic Supernova*, arXiv:1306.0559 [astro-ph.HE] (2013)

[30] K. S. Babu et al. - *Baryon Number Violation*, arXiv:1311.5285 [hep-ph] (2013)

[31] G. Lutter - *A new versatile underground gamma-ray spectrometry system*, Appl. Radiat. Isot. **81**, 81 (2013)

[32] K. Abe et al. (SK collaboration) - *Search for Proton Decay via $p \to \nu K^+$ using 260 kiloton·year data of Super-Kamiokande*, Phys. Rev. D **90**, 072005 (2014)

[33] N. Soppera, M. Bossant, E. Dupont - *JANIS 4: An Improved Version of the NEA Java-based Nuclear Data Information System*, Nuclear Data Sheets, **120**, 294-296 (2014)

[34] T. J. Irvine - *Development of Neutron-Tagging Techniques and Application to Atmospheric Neutrino Oscillation Analysis in Super-Kamiokande*. University of Tokyo, doctoral thesis (2014)

[35] A. Renshaw (SK collaboration) - *First Indication of Terrestrial Matter Effects on Solar Neutrino Oscillation*, Phys. Rev. Lett. 112, 091805 (2014)

[36] K. Abe et al. (SK collaboration) - *Limits on sterile neutrino mixing using atmospheric neutrinos in Super-Kamiokande*, Phys. Rev. D **91**, 052019 (2015)

[37] L. Labarga - *Discovery of Neutrino Oscillations, the experimental program*, Departamento de Física Teórica UAM (2015)

[38] K. Abe et al. (SK collaboration) - *Search for $n - \bar{n}$ oscillation in Super-Kamiokande*, Phys. Rev. D **91**, 072006 (2015)

[39] K. Abe et al. (SK collaboration) - *Test of Lorentz Invariance with Atmospheric Neutrinos*, Phys. Rev. D **91**, 052003 (2015)

[40] S. M. Bilenky - *Neutrino in Standard Model and beyond*, arXiv:1501.00232 [hep-ph] (2015)

[41] K Choi et al. (SK collaboration) - *Search for neutrinos from annihilation of captured low-mass dark matter particles in the Sun by Super-Kamiokande*, arXiv:1503.04858 [hep-ex] (2015)

[42] F. Deppisch, P. S. Bhupal Dev, A. Pilaftsis - *Neutrinos and Collider Physics*, New J. Phys. **17** 075019 (2015)

[43] S. W. Li, J. F. Beacom - *Spallation backgrounds in Super-Kamiokande are made in muon-induced showers*, arXiv:1503.04823 [hep-ph] (2015)

[44] R. B. Patterson - *Prospects for measurement of the neutrino mass hierarchy*, Ann. Rev. of Nucl. and Part. Sci. **65**, 177 (2015)

[45] K. Abe et al. (SK collaboration) - *Solar Neutrino Measurements in Super-Kamiokande-IV*, arXiv:1606.07538 [hep-ex] (2016)

[46] P. Fernandez - *Gd-doping and the impact on Super Kamiokande and T2K*, NNN16, Beijing (2016)

[47] S. Dell'Oro, S. Marcocci, M. Viel, F. Vissani - *Neutrinoless Double Beta Decay: 2015 Review*, Adv. High Energy Phys. **2016**, 2162659 (2016)

[48] A. Ianni - *Canfranc Underground Laboratory*, J. Phys.: Conf. Ser. **718** 042030 (2016)

[49] T. J. Winchester - *A search for hep solar neutrinos at the Sudbury Neutrino Observatory*, University of Washington, PhD dissertation (2016)

[50] K. Abe et al. (SK collaboration) - *Search for Proton Decay via* $p \to e^+\pi^0$ *and* $p \to \mu^+\pi^0$ *in* 0.31 *megaton·years exposure of the Super-Kamiokande Water Cherenkov Detector*, Phys. Rev. D **95**, 012004 (2017)

[51] P. Fernández - *Neutrino Physics in Present and Future Kamioka Water-Cherenkov Detectors with Neutron Tagging*. Universidad Autónoma de Madrid, doctoral thesis (2017)

[52] J. Pérez - *Radioactive Contamination in Neutrino Experimental Physics: the Cases of NEXT and Super-Kamiokande Experiments*. Universidad Autónoma de Madrid, doctoral thesis (2017)

[53] K. Abe et al. (SK collaboration) - *Atmospheric neutrino oscillation analysis with external constraints in Super-Kamiokande I-IV*, Phys. Rev. D **97**, 072001 (2018)

[54] K. Abe et al. (HK proto-collaboration) - *HyperK design report*, arXiv:1805.04163 [physics.ins-det] (2018)

[55] F. Capozzi, S. W. Li, G. Zhu, J. F. Beacom - *DUNE as the Next-Generation Solar Neutrino Experiment*, Phys. Rev. Lett. **123**, 131803 (2019)

[56] S. R. Choudhury, S. Choubey - *Updated Bounds on Sum of Neutrino Masses in Various Cosmological Scenarios*, JCAP, **09**, 017 (2018)

[57] I. Esteban et al. (nu-fit.org) - *Global analysis of three-flavour neutrino oscillations: synergies and tensions in the determination of* θ_{23}*,* $\delta_{\rm CP}$*, and the mass ordering*, JHEP, **01**, 106 (2019)

[58] Kachulis et al. (SK collaboration) - *Search for Boosted Dark Matter Interacting With Electrons in Super-Kamiokande*, Phys. Rev. Lett. **120**, 221301 (2018)

[59] M. Shiozawa - *Proton decay and* $n-\bar{n}$ *oscillations with SK(-Gd), DUNE, Hyper-K, and JUNO*. European Neutrino Town meeting, CERN (2018)

[60] K. Abe et al. (T2K collaboration) - *Constraint on the Matter-Antimatter Symmetry-Violating Phase in Neutrino Oscillations*, Nature **580** 339 (2020)

[61] Abe et al. (T2K collaboration) - *Search for light sterile neutrinos with the T2K far detector Super-Kamiokande at a baseline of 295 km*, Phys. Rev. D **99**, 071103 (2019)

[62] M. Jiang et al. (SK collaboration) - *Atmospheric Neutrino Oscillation Analysis With Improved Event Reconstruction in Super-Kamiokande IV*, Prog. Theor. Exp. Phys. (2019)

[63] P.A. Zyla et al. - PDG Ch. 14 - *Neutrino Masses, Mixing and Oscillations*, Prog. Theor. Exp. Phys. **2020**, 083C01 (2020)

[64] P.A. Zyla et al. - PDG Ch. 25 - *Neutrinos in Cosmology*, Prog. Theor. Exp. Phys. **2020**, 083C01 (2020)

[65] P.A. Zyla et al. - PDG Ch. 61 - *Light neutrino types from collider searches*, Prog. Theor. Exp. Phys. **2020**, 083C01 (2020)

[66] K. Abe et al. (SK collaboration) - *Search for Electron Antineutrino Appearance in a Long-baseline Muon Antineutrino Beam.* Phys. Rev. Lett. **124**, 161802 (2020)

[67] K. Abe et al. (SK collaboration) - *Indirect Search for Dark Matter from the Galactic Center and Halo with the Super-Kamiokande detector*, arXiv:2005.05109 [hep-ex] (2020)

[68] M. Tanaka et al. (SK collaboration) - *Search for proton decay into three charged leptons in 0.37 megaton-years exposure of the Super-Kamiokande*, Phys. Rev. D **101**, 052011 (2020)

[69] Ll. Marti et al. - *Evaluation of Gadolinium's Action on Water Cherenkov Detector Systems with EGADS*, Nucl. Instrum. Methods Phys. Res. **959**, 163549 (2020)

[70] G. Ranucci - *First detection of solar neutrinos from CNO cycle with Borexino*, Neutrino2020 (2020)